2006-12

A first report on electromigration studies at a model copper-aluminum railgun contact

Delaney, Luc D.

Monterey, California. Naval Postgraduate School

NAVAL POSTGRADUATE SCHOOL

MONTEREY, CALIFORNIA

THESIS

A FIRST REPORT ON ELECTROMIGRATION STUDIES AT A MODEL COPPER-ALUMINUM RAILGUN CONTACT

by

Luc D. Delaney

December 2006

Thesis Advisor: Indranath Dutta

Approved for public release; distribution is unlimited

THIS PAGE INTENTIONALLY LEFT BLANK

REPORT DOCUMENTATION PAGE			Form Approved OMB No. 0704-0188
Public reporting burden for this collection of information is estimated to average 1 hour per response, including the time for reviewing instruction, searching existing data sources, gathering and maintaining the data needed, and completing and reviewing the collection of information. Send comments regarding this burden estimate or any other aspect of this collection of information, including suggestions for reducing this burden, to Washington headquarters Services, Directorate for Information Operations and Reports, 1215 Jefferson Davis Highway, Suite 1204, Arlington, VA 22202-4302, and to the Office of Management and Budget, Paperwork Reduction Project (0704-0188) Washington DC 20503.			
1. AGENCY USE ONLY *(Leave blank)*	**2. REPORT DATE** December 2006	**3. REPORT TYPE AND DATES COVERED** Master's Thesis	
4. TITLE AND SUBTITLE : A First Report on Electromigration Studies at a Model Copper-Aluminum Railgun Contact.		**5. FUNDING NUMBERS**	
6. AUTHOR(S) Luc D. Delaney			
7. PERFORMING ORGANIZATION NAME(S) AND ADDRESS(ES) Naval Postgraduate School Monterey, CA 93943-5000		**8. PERFORMING ORGANIZATION REPORT NUMBER**	
9. SPONSORING /MONITORING AGENCY NAME(S) AND ADDRESS(ES) N/A		**10. SPONSORING/MONITORING AGENCY REPORT NUMBER**	
11. SUPPLEMENTARY NOTES The views expressed in this thesis are those of the author and do not reflect the official policy or position of the Department of Defense or the U.S. Government.			
12a. DISTRIBUTION / AVAILABILITY STATEMENT Approved for public release; distribution is unlimited.		**12b. DISTRIBUTION CODE** A	

13. ABSTRACT (maximum 200 words)

The purpose of this thesis was to develop an experimental methodology to determine the effects of electromigration on the aluminum microstructure of the railgun armature. An experimental system which allowed simulation of an Al armature between two Cu rails with surface "skins" was devised. The system was designed small enough such that only small current (<10A) was necessary to produce the large current densities typically found in railguns, and was able to simulate the skin effect on both the Cu rails and Al armature under static, long-term testing conditions. In this method, the effects of electromigration were discerned clearly, in dissociation from various movement related damage phenomena. The aluminum from the armature quickly reached its melting point via Joule heating due to high contact resistance at the armature-rail contact. Once liquid aluminum was formed, it rapidly migrated along the copper rail towards the negative terminal. This transport of liquid aluminum along the copper rails was attributed to electromigration of the liquid under the influence of the direct electric field. Once the aluminum began to be transported along the rail towards the cathode terminal, it alloyed with the copper rails and the resistance steadily increased in the circuit. Electromigration is shown to be a contributing factor to the degradation of aluminum armatures performance and copper rails lifespan in the railgun.

14. SUBJECT TERMS Railgun, Electromigration, Current Density, Thin Films			**15. NUMBER OF PAGES** 71
			16. PRICE CODE
17. SECURITY CLASSIFICATION OF REPORT Unclassified	**18. SECURITY CLASSIFICATION OF THIS PAGE** Unclassified	**19. SECURITY CLASSIFICATION OF ABSTRACT** Unclassified	**20. LIMITATION OF ABSTRACT** UL

NSN 7540-01-280-5500

Standard Form 298 (Rev. 2-89)
Prescribed by ANSI Std. 239-18

THIS PAGE INTENTIONALLY LEFT BLANK

Approved for public release; distribution is unlimited

A FIRST REPORT ON ELECTROMIGRATION STUDIES AT A MODEL COPPER-ALUMINUM RAILGUN CONTACT

Luc D. Delaney
Lieutenant, United States Navy
B.S., United States Naval Academy, 1999

Submitted in partial fulfillment of the
requirements for the degree of

MASTER OF SCIENCE IN MECHANICAL ENGINEERING

from the

NAVAL POSTGRADUATE SCHOOL
December 2006

Author: Luc D. Delaney

Approved by: Indranath Dutta
Thesis Advisor

Anthony J. Healey
Chairman, Department of Mechanical and Astronautical Engineering

THIS PAGE INTENTIONALLY LEFT BLANK

ABSTRACT

The purpose of this thesis was to develop an experimental methodology to determine the effects of electromigration on the aluminum microstructure of the railgun armature. An experimental system which allowed simulation of an Al armature between two Cu rails with surface "skins" was devised. The system was designed small enough such that only small current (<10A) was necessary to produce the large current densities typically found in railguns, and was able to simulate the skin effect on both the Cu rails and Al armature under static, long-term testing conditions. In this method, the effects of electromigration were discerned clearly, in dissociation from various movement related damage phenomena. The aluminum from the armature quickly reached its melting point via Joule heating due to high contact resistance at the armature-rail contact. Once liquid aluminum was formed, it rapidly migrated along the copper rail towards the negative terminal. This transport of liquid aluminum along the copper rails was attributed to electromigration of the liquid under the influence of the direct electric field. Once the aluminum began to be transported along the rail towards the cathode terminal, it alloyed with the copper rails and the resistance steadily increased in the circuit. Electromigration is shown to be a contributing factor to the degradation of aluminum armatures performance and copper rails lifespan in the railgun.

THIS PAGE INTENTIONALLY LEFT BLANK

TABLE OF CONTENTS

THIS PAGE INTENTIONALLY LEFT BLANK

LIST OF FIGURES

LIST OF TABLES

THIS PAGE INTENTIONALLY LEFT BLANK

ACKNOWLEDGMENTS

I would like to thank my advisor, Professor Indranath Dutta, for his guidance and encouragement throughout this project. I would like to thank Chadee Persad, Ramesh Guduru, Tiandan Chen, Chanman Park and Tom Christian for contributing their time and expertise. Finally, I would like to thank my wife, Asako, and daughter, Maya, for their love, patience and support.

This research was supported by the Office of Naval Research MURI Grant # N00014-04-1-0599RQ-M.

THIS PAGE INTENTIONALLY LEFT BLANK

I. INTRODUCTION

A. RAILGUN

The U.S. Navy currently employs conventional guns, missiles, and aircraft in conducting land attack operations. Conventional guns are very affordable and can be used repeatedly for long durations with little wear or damage to equipment on board ship. They are very effective in saturating targets near the shoreline. The down side to conventional guns is that their range is very limited compared to the battlespace geography encountered in today's conflicts. Missiles and aircraft have the range needed to reach targets deep inland from the shore, but are extremely expensive to use and therefore cannot be employed in enough volume to saturate a battlespace with suppressive fire.

The United States Navy has begun to commit substantial research efforts to the development of an electromagnetic (EM) railgun for use onboard ships. This railgun would ideally be capable of landing 60 kg projectiles 300 to 400 nautical miles downrange with an impact velocity of up 2.5 km/s [1]. This weapon would close the gap between conventional, low cost, guns and precision, long range, high cost, missiles and aircraft ordnance [2, 3].

The railgun operates by passing a large pulsed current, likely in excess of several million amperes [2] depending on armature weight, along a rail which is usually made of copper. The current then flows in to an armature made of aluminum and out on to another copper rail that is set parallel to the first. The large current causes a Lorentz force to push the armature along the rails, see Figure 1. In laboratory experiments the armature has been ejected from the rail system at speeds up to 6 km/s [4, 5]. The Lorentz equation used to calculate the force on the armature is:

$$F_{EM} = \tfrac{1}{2} L' \bar{I}^2 \quad \textbf{Equation 1}$$

Where L' is the inductance gradient of the barrel and I is the average current.

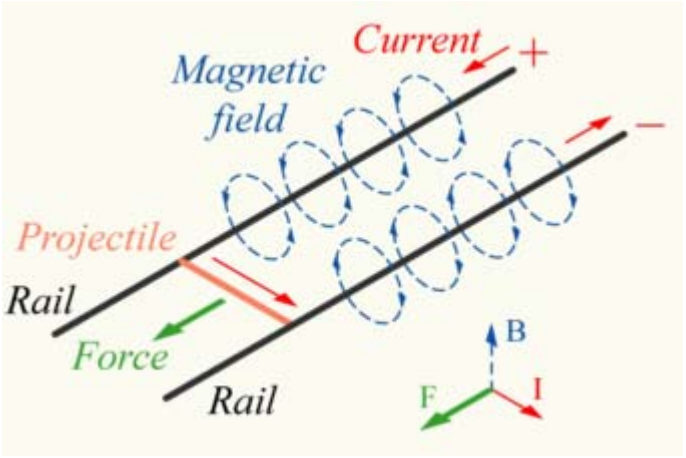

Figure 1. A conceptual representation of the current and resulting force on a projectile (armature) in a railgun. ([From Ref. [6].)

Several types of materials for the armature are being explored namely aluminum, copper, and alloys of the two. The most common armature composition for the experimental railgun is aluminum 7075.

B. PROBLEMS WITH CURRENT RAILGUN TECHNOLOGY

There have been several obstacles in the development of an operational railgun system. These problems are in two areas; the first being power supply and the second is rail/armature damage. The primary concern with power supply is the associated equipment required to support the rapid electrical discharge required to launch a railgun armature. The support equipment requires ample power generation and storage facilities. This makes a small and portable system harder to implement.

Damage to the rail and armature is another concern that has several components. As the armature is propelled along the rails several problems have been observed. Hypervelocity gouging of the rails from the aluminum armature has been observed [7, 8]. Also melt-wave erosion of the armature occurs from the joule heating and melting of the armature [9-11]. Viscous heating from the friction of the armature passing along the rails causes melting and deposition of the aluminum on the rails [12]. Also observed was crack propagation due to the large current density passing through the armature and

propagating existing crack initiation sites [13]. Lastly, electromigration and flow of the aluminum armature is an effect that will be discussed in this study.

C. PURPOSE OF STUDY

As stated in the previous paragraphs there are several factors that result in damage to both the rails and armature. Examination of effects other than from movement of the armature has been difficult to observe and analyze due to the multiple artifacts that arise due to high velocity motion of the armature. The purpose of this thesis was to utilize a small scale, static model of a rail gun to examine the effects of electromigration on the railgun armature. The testing examined the effects of passing a large current density along simulated copper rails and through an armature composed of 1100 Aluminum. The static model allowed for analysis of the effect of strictly the current flow through the rails and armature.

THIS PAGE INTENTIONALLY LEFT BLANK

II. BACKGROUND

A. LITERATURE REVIEW ON RAIL/ARMATURE DAMAGE IN RAILGUN

There are several issues involving the railgun armatures that have prevented the implementation of this technology. The most commonly observed problems are hypervelocity gouging, melt-wave erosion and viscous heating wear. The damage caused by these problems limits the useable lifespan of the rails and reduces the performance of the propulsion armature.

The most easily recognizable problem is gouge marks in the copper rails that are formed as the armature slides past the rail. This damage is often very severe and limits the lifespan of the rails. Several methods of gouging have been explored. Experimentation has shown the most likely cause of gouging results from particles resting on the rail in the path of the armature. The pressures developed by the speed of the armature exceed the yield strength of both armature and rail material and result in craters and bumps. These bumps then tear the soft rail material leaving a gouge in the rail. The initiation of the gouge leads to even more significant damage on subsequent shots. The most significant damage via gouging has been observed at armature speeds of 1.5-2.5 km/s [7, 8].

Another possible method of gouging that has seen little experimental observation is gouging by high velocity molten aluminum. It is possible that as molten aluminum from the armature falls and impacts the rails at high speed, it causes gouging. It has been difficult to correlate this type of gouging to molten aluminum since aluminum residue is not necessarily left behind at the gouge site. However, other methods of aluminum deposition on to the rails have been observed and will be discussed below. The deposition of aluminum gives future sites for “particle” gouging to initiate on subsequent shots [7].

Another form of damage in railgun armatures is known as melt-wave erosion. This occurs as a result of a combination of high current densities passing through the armature edge and the high velocity of the armature along the rail. As the current moves from the

rail to the edge of the armature the current densities cause this armature material to melt. In a rail gun the armature is propelled forward along the rail and the molten armature is removed via viscous entrainment. As the armature is removed a gap is formed and the current is forced forward on the armature. The process repeats itself in a "wave" fashion until it reaches the front of the armature. Once the front of the armature is eroded the gap causes a spike in voltage and arcing occurs [9, 10]. This process reduces the efficiency and effectiveness of the armature. Experimental results have shown that with the right combination of metals and current density a single shot can yield up to 0.5 mm of melt-wave erosion in the armature [11]. This form of erosion also leaves significant amounts of melted metal from the armature on the rails which will cause gouging damage on subsequent passes.

Melting of the armature also occurs via viscous heating. The friction of the armature sliding along the rail causes the armature to melt and form a molten film which is predominately left behind as the armature progresses along the rail [12]. This leads to problems similar to those noted above with melt-wave erosion.

The last form of damage that has been explored thus far is a result of pulsed electromagnetic loading in the armature. The damage is crack tip propagation that results in the armature from pulsed electromagnetic loading. It has been shown that at large current densities the cracks will propagate from initiation points in the microstructure. At even larger current loads small blowholes have been observed as a result of localized melting in the armature [13].

B. CURRENT CROWDING AND SKIN EFFECTS

The research conducted by Chen et al. [14] examined the effect of current crowding observed in the corner regions of armatures where the current first passes from the rail to the armature. The effect is reduced in situations where the armature is fixed and cannot move. However, as speed is introduced in to the characteristics of the armature current crowding becomes a significant issue. The current experiences a skin effect where it travels along the outer surface of the rail and crowds in the aluminum armature at the

corner where the rail and armature meet. This crowding is observed at both the inlet and outlet of the armature. The current crowding was observed to cause localized melting and crack propagation at crack initiation sites in the crowding region [14-17].

C. ELECTROMIGRATION

The role of electromigration in railguns has not been investigated previously. Electromigration is the atomic transport of metals under the influence of an electric field. This phenomenon has been observed since as early as 1861 when Geradin first observed this movement in lead-tin and mercury-sodium alloys [18]. Systematic experimentation was begun in the early 1950s and by the late 1960's research in the area of thin films was conducted by Blech [18-22] and the first real micro scale observation of electromigration damage was seen.

In his research, Black [23] found that metal ions can be set free in their lattice by thermal activation. Once this occurs they will become subject to opposing forces; the "electric wind" force acted on the ion cores by electrons pushing the ions towards the anode, and the electric field, or "direct force", induced by the positive current pushes the ions towards the cathode. The prevailing force is dependent on the type of metal, thickness, and current density. The result is the ability to quantify electromigration and the median time to failure in small scale semiconductors as expressed in the following formula [23]:

$$\frac{1}{MTF} = AJ^2 \exp - \frac{\phi}{kT} \quad \textbf{Equation 2}$$

Where MTF is the median time to failure in hours, A is the cross sectional area of the device (cm^2), J is the current density (A/cm^2), φ is the activation energy (eV), k is the Boltzman's constant ($1.38x10^{-3}$J/K) and T is the temperature (^oK).

Blech's research in thin films showed that it was possible to model the atomic drift speed of atoms by using the following formula [20]:

$$v = \frac{J}{N} = \frac{D_o}{kT} eZ^* \rho j \exp\left(-\frac{\Delta H}{kT}\right) \textbf{ Equation 3}$$

Where J is the atom flux (moles/m^2s), N is the density of metal ions (moles/m^2), D_O is the frequency factor for diffusion (m^2/s), k is the Boltzmann's constant ($1.38x10^{-3}$J/K), T is the absolute temperature, eZ^* is the effective charge, ρ is the resistivity (Ω-cm), j is the current density (A/cm^2), and ΔH is the activation energy (J) for moving defects in the metal. The most relevant part of the above equation is the atom flux, J, which can be calculated by:

$$J = \frac{ND}{kT} Z^* eE \textbf{ Equation 4}$$

where is the electronic charge and E is the electric field. The diffusion coefficient, D, is given by:

$$D = D_o \exp\left(-\frac{\Delta H}{kT}\right) \textbf{ Equation 5}$$

Blech's research determined that current densities must achieve at least 10^4 A/cm^2 in order for electromigration to occur in thin films. However, once the threshold of 10^5~10^6 A/cm^2 current densities is crossed electromigration becomes much more rapid and the effects much more severe. Blech determined that inputs from temperature, current density, specimen geometry, and material composition will all have some contribution to the magnitude of electromigration [19]. Blech's research showed that the flow of thin film metals is always in the direction of electron flow since the influence of the "wind force" typically dominates over that of the "direct force".

D. ELECTROMIGRATION RELATED DAMAGE IN MICROELECTRONIC CONTACTS

Another area of electromigration research, and where conceptual modeling for this thesis came from, has been in solder joints and interconnects [24]. In the research conducted by Lin et. al., it was observed that failure of flip-chip solders can occur under conditions with current densities as low as 10^4 A/cm^2 due to their bulk properties [25]. The reason for degradation at low current densities is the high resistivity, small Young's modulus and high effective charge of solders (eg. Pb or Sn) when compared with aluminum interconnects.

The failure of these interconnects usually resulted from the formation and propagation of a void in the solder joint. The results of ref. 24 showed that current crowding played a large role in the formation of voids and degradation of the solder joints. Current crowding was affected by the current path which was influenced by the sample design. The current crowding in small cross sectional areas, such as corners, yielded high current densities which caused localized melting, due to Joule heating, formation and propagation of voids and resulted in joint failure. As the experiments progressed void propagation decreased the cross sectional area for current to pass which exacerbated the effects of electromigration and rapidly moved to sample to failure. The results of ref. 24 clearly showed the impact of high current densities and current crowding on metals.

E. ELECTROMIGRATION IN LIQUIDS

Another aspect of electromigration that is of significant interest to this study is its characteristics in metals while in the liquid state. Research conducted by Anthony [26] addressed the electromigration of several liquid metal inclusions in single crystal silicon. Metal inclusions were embedded in the silicon by ultrasonically drilling a 0.75 mm diameter hole in the substrate. A 0.70 mm diameter metal wire was then place in the hole and the sample was placed in an annealing furnace at 1100^o C for three hours in order to form the liquid alloy inclusion.

Inclusions in single crystal silicon were observed to migrate toward either the anode or cathode based on the influence of the electric current. The applied current caused the liquid metal inclusions to absorb dissolving silicon atoms which were then transported through the inclusion and deposited on the other side via flux. The cause of the flux is due a combination of the "electric wind" force, the electric field force, and thermal gradient migration. The predominant force acting in these samples was determined by the solubility of silicon in the metal inclusion and the charge of the silicon.

In this research it was observed that aluminum in the liquid state will migrate towards the cathode. It was observed that liquid aluminum is one of the easiest metals to initiate electromigration in this environment due to the high solubility of silicon in aluminum. The dissolved silicon was pushed by the "electric wind" force towards the anode and deposited. This allowed the aluminum to migrate towards the cathode aided by the direct electric field force.

Other research on electromigration in liquid alloys conducted by Epstein et al. [27] reinforced the influence of an "electron drag" force. This force is caused by the interaction of the electrons passing through, causing a "wind force", but hitting the ions in the liquid which flow the opposite direction resulting in a resistance, or "drag", on these ions. The research was conducted on alloys consisting of several metals, solutes, mixed with mercury, the solvent. The result is a drift velocity of the solute which is separated from the solvent based on the ion cross section in the liquid and determines the direction of flow for the solutes.

Previously stated research dealt with the electromigration of liquids in alloy metals or as interstitials. However, more relevant research was conducted by Regan et al. [28] on the use of carbon nanotubes as mass conveyors. The research investigated the movement of single element liquid balls of indium. The research was done at a nanoscale, however, its implications are far reaching and apply to this current study. The research placed nanoparticles of indium on carbon nanotubes and applied a current to the system. Joule heating quickly raised the temperature of the indium to above the melting temperature. Once molten the indium moved with the current in the direction of the

cathode. This result was confirmed by reversing the current and witnessing the indium move again towards the new cathode. The mass transfer rate could be controlled by varying the voltage applied. The transport of the indium particles, which are resting on top of the nanotubes, has been attributed to the "direct" force induced by the current. This seems to be the most plausible explanation; however, the authors state that more work needs to be done for a full understanding of the mechanisms involved in the mass transport.

F. SURFACE ELECTROMIGRATION

Electromigration experiments on semiconductor surfaces have shown that the flow of metals in electromigration may, under certain conditions, be in either the direction of electron flow or against the electron flow. In a very thin layer of metal (a couple of monolayers), electromigration has been seen in a direction opposite to that of electron flow. This is called surface electromigration. Research conducted by Yasunga and Notori [29] showed a variety of results for surface electromigration on silicon substrates.

In these experiments sample metals were deposited on silicon substrates with a thickness between one and ten monolayers. Current was then applied to the substrate which heated the metal to near its melting temperature. This heating increased the mobility of the metal atoms and promoted the electromigration process. Surface electromigration occurs in the top layer of metals where the atoms are more loosely packed, and surface diffusion, which is much faster than grain boundary diffusion, dominates. The current densities required are therefore much less than in bulk of thin film electromigration experiments when considering the added mobility from Joule heating. Yasunga and Notori [29] showed that surface electromigration may occur at current densities as low as 10 A/cm^2.

In conventional electromigration, bulk or thin film, the electric wind component of the effective charge is a large negative value. The "direct" force value is near unity and thus the dominant driving mechanism is the "wind force". Conventional electromigration

also requires large current densities to operate as previously discussed. However, on the surface layer of metals where the atoms are freer to diffuse than in the bulk, the driving mechanism may be switched. When a low current density is applied the force on the atoms by the "wind force" is small relative to that of the electrostatic "direct" force. When the mobility of the metal ions on the surface is increased due to Joule heating flow of metals ions will commence and tend towards the cathode [30-32].

The total force acting on an atom is comprised of the effective charge number, Z*, the elementary charge, q, and the electric field, E, shown in the following equation [29, 32]:

$$F = Z^* qE \text{ . } \textbf{Equation 6}$$

The effective charge number, Z*, is further broken in to the electrostatic, Z_{el}, and wind, Z_w, parts:

$$Z^* = Z_{el} + Z_w \text{ . } \textbf{Equation 7}$$

As indicated in ref. 29, the direction of surface electromigration can vary for different metals, but the predominant tendency is for atom flow to be towards the cathode. The flow direction for different sample types is summarized in Table 1.

Another difference in the mechanisms between conventional and surface electromigration is the resultant microstructure. Conventional electromigration causes pits and voids to form on the cathode side of the metal and hillocks to form towards the anode. This results in a damaged microstructure that is weakened structurally and has increased resistivity. The result of surface electromigration is the growth of a layer towards the cathode. The movement is more fluid in nature, transporting the top layer as a system and not in segments. Therefore, although there is structural change there is less in the way of microstructure damage.

The conclusion of ref. 29 is that surface electromigration is the result of the "direct" force from an applied current that overcomes the effect of the "electron wind" force from the electron flow in situations where atoms are loosely attached to the bulk and therefore highly mobile.

Properties	Electromigration		
Direction of Flow	In Bulk	In Film	Semiconductor Surface
Al	anode	anode	anode or cathode
Ag	anode	anode	cathode
Au	anode	anode	anode
In	anode	anode	cathode
Sn	anode	anode	cathode
Current Density (A/cm^2)	10^4	10^6	10
Electric Field (V/cm)	10^{-2}	1	10

Table 1. Comparison of electromigration properties (After Ref. [29])

THIS PAGE INTENTIONALLY LEFT BLANK

III. OBJECTIVE

The objective of this thesis was to develop an experimental procedure to evaluate the effects of electromigration in railgun armatures. A model experimental system, which allows simulation of an Al armature between two Cu rails with surface "skins", was devised to meet two key requirements. They are 1) the overall system must be small enough such that only small current (<10A) are necessary to produce the large current densities typically found in railguns, and 2) the system must enable simulation of the skin effect on both the Cu rails and Al armature even under static, long term testing conditions, so that the effects of electromigration can be discerned clearly, in dissociation from various movement related damage phenomena. The first step was to develop an apparatus with suitable environment control in which to conduct testing in. The second step was to integrate necessary wiring systems needed to meet power supply requirements and to record voltage and temperature measurements. The next step was to develop a fabrication process, which could easily be replicated, and to build suitable specimens for evaluation. Once the system and samples were fabricated the experiments were conducted to examine whether the armatures suffered any damage, and if so, if it was attributable to electromigration.

THIS PAGE INTENTIONALLY LEFT BLANK

IV. EXPERIMENTAL PROCEDURE

A. DESIGN OF SIMULATED STATIC RAILGUN FOR EM EXPERIMENTS

The experimental phase of this research was composed of system design, procurement, sample preparation and testing. It was imperative that the experiments be conducted in an atmosphere that would prevent oxidation of the copper rails in order to accurately gauge the effect of electromigration damage to the armature. As the electromigration damage progressed, the resistance of the armature increased and was measured. Initial testing was conducted placing sample copper rail in to the furnace and heating the sample to 480^{o} C. The environment was washed with a constant positive pressure of Ar/H_2 (98%/2%) gas to inert the environment. Results of this testing indicated that minor oxidation of the copper rails was still occurring and that a vacuum environment would be required for future experimentation.

1. System Design and Components

The experimental system required a furnace that could be placed under vacuum. The system needed to have an electrical feedthrough which was capable of wiring to supply power and measure temperature and voltage. For this, a tube furnace with working dimensions of approximately six inches in diameter by four feet in length was utilized. It had a heated length of approximately 18 inches. The furnace controller was a Thermcraft type 815. It was capable of programming up to nine different dwell temperature rates and had controllable ramp rates. The tube furnace was modified to accept a vacuum pump. A Pfeifer-Balzers TPU 240 turbomolecular pump was integrated into the system. The turbomolcular pump was able to produce a vacuum of $4x10^{-4}$ torr.

An electrical feedthrough was installed on to the endcap of the furnace and fitted with connections for a power supply, nanovoltmeter, and thermocouple as shown in Figure 2. An Agilent E3632A power supply capable of producing up to 30 volts and 15 amperes of current was integrated with the system. The power supply had a dual readout display which indicated both voltage and current applied. An Agilent 34420A nanovoltmeter with sensitivity to 100pV was also integrated into the system. The

thermocouple connection was connected to an Omega, K-type, thermocouple gauge. On the opposite end cap of the electrical feedthrough and gas connection had been previously installed and was connected to the AR/H_2 gas supply. This allowed the furnace to be filled with inert gas prior to turning on the vacuum pump and added an extra measure in purifying the environment inside the furnace.

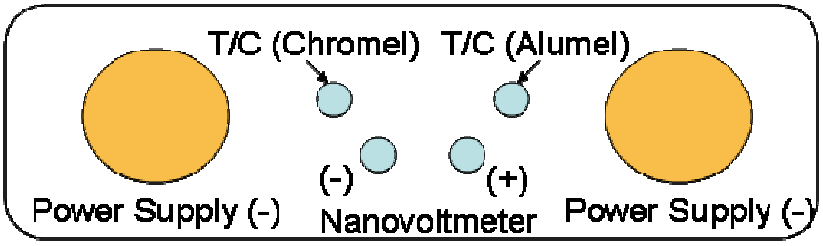

Figure 2. Schematic of electrical feedthrough layout.

The power supply and nanovoltmeter were connected to a desktop computer and interfaced with the Microsoft Excel™ program. An Excel™ toolbar specifically designed for the power supply enabled the output of the power supply to be controlled from the computer. The toolbar also setup a data logging spreadsheet which recorded the voltage and current output for the power supply at intervals as little as one second. Figure 3 is a picture of the vacuum furnace and the cart which held the computer, power supply, nanovoltmeter, and vacuum gauge controller. Figure 4 shows a schematic of the system design.

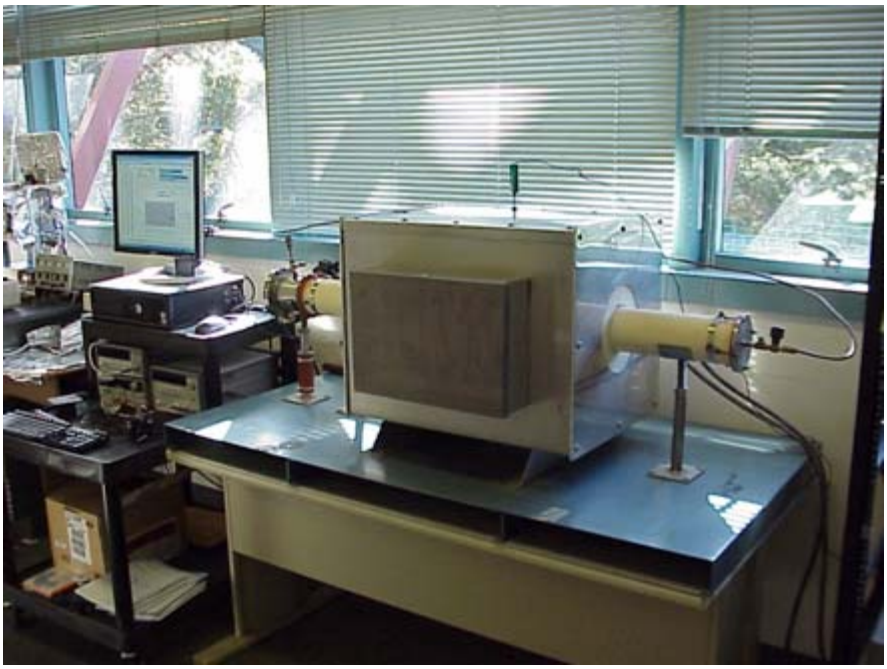

Figure 3. Picture of tube furnace and associated data logging computer.

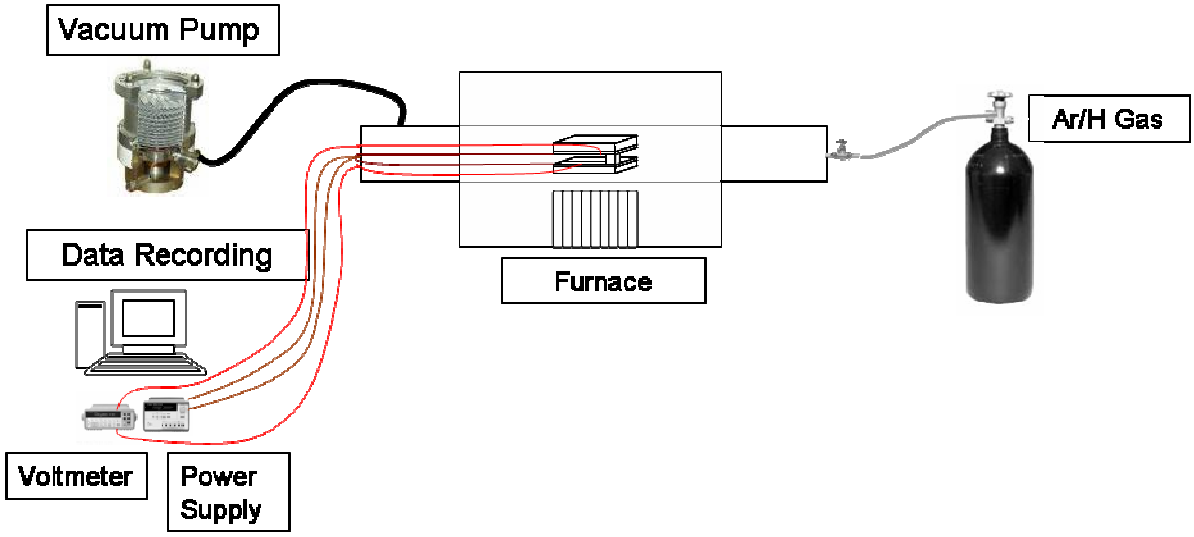

Figure 4. Schematic of furnace, power supply, vacuum and gas setup.

2. Armature and Rail Construction

The rail samples were constructed using a silicon wafer that had 1 μm of copper deposited on the surface. There was a 70 nm thick tantalum nitride barrier between the silicon and copper to prevent the copper from diffusing into the silicon substrate. The wafer was cut using a diamond blade and individual samples measuring 40 mm long by 6.7 mm wide were made. The copper rails were then made by placing a 1 mm wide strip of 1mil (25 μm) Kapton tape along the long edge of copper samples as shown in Figure 5. This enabled the Kapton tape to mask the underlying copper from subsequent etching. The Kapton tape was placed on both long edges of the sample in order to produce two rails to compare the copper rails with and without current passed through. The copper samples were placed in a solution of 3 grams of $Na_2S_2O_8$ and 3% H_2SO_4 in 1000 ml of H_2O. The samples and solution were placed in agitation for approximately three minutes until the exposed copper had been etched off. The sample were rinsed in DI water and dried. The Kapton tape was removed and rail preparation was complete.

Armature samples were made using quartz blocks and aluminum 1100 foil. The foil thickness used for these experiments was approximately 76 micrometers. The foil was cut into 1 mm wide strips to match the approximate width of the copper rails. The foil was wrapped around three sides of the quartz block which measured 11 mm long and 3 mm thick as shown in Figure 6. The length of the aluminum on the top and bottom sides of the quartz were not for conducting purposes, but simply for holding the foil between the two rails in place. Alternative methods of adhering just one side of aluminum between the two copper rails were attempted, but proved to be too difficult to work with on this scale.

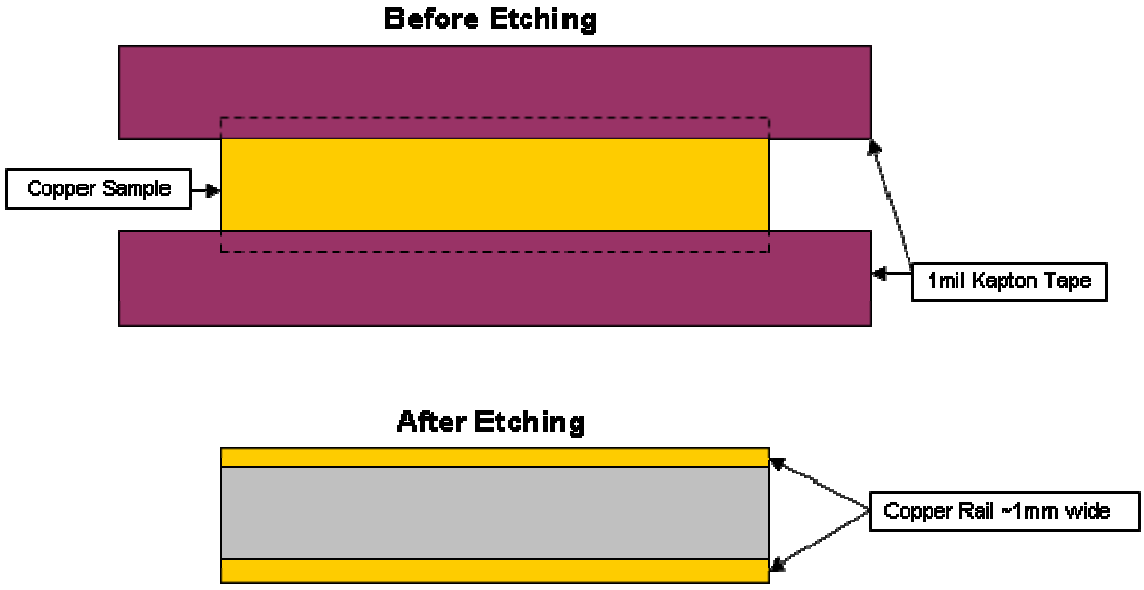

Figure 5. Etching of Copper plated Silicon plate using Kapton tape.

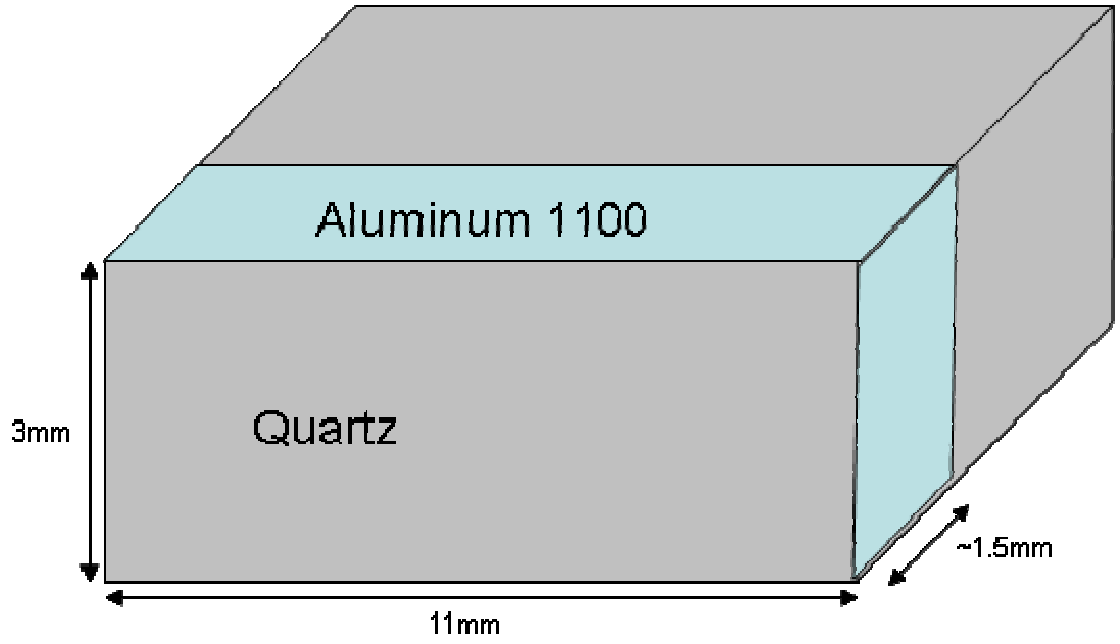

Figure 6. A Schematic of 100μm thick Al 1100 (Not to Scale) wrapped around a non-conducting Quartz block.

The armature test piece was then placed between two rail samples. The test pieces were placed in a manner such that the aluminum strip overlapped one of the copper rails on each silicon sample as depicted in Figure 7. The rails sandwiched the aluminum on the top and bottom of the quartz and held the test piece together via a compression clamp. The clamp used was an office supply binder clip from which the paint was stripped down to expose its steel core. The clips gave substantial compression force at room temperature. It was seen that after each experiment the clips became weakened because of the heat treatment. The clips still maintained adequate compressive force to maintain contact, but it was reduced and the clips could be used only once.

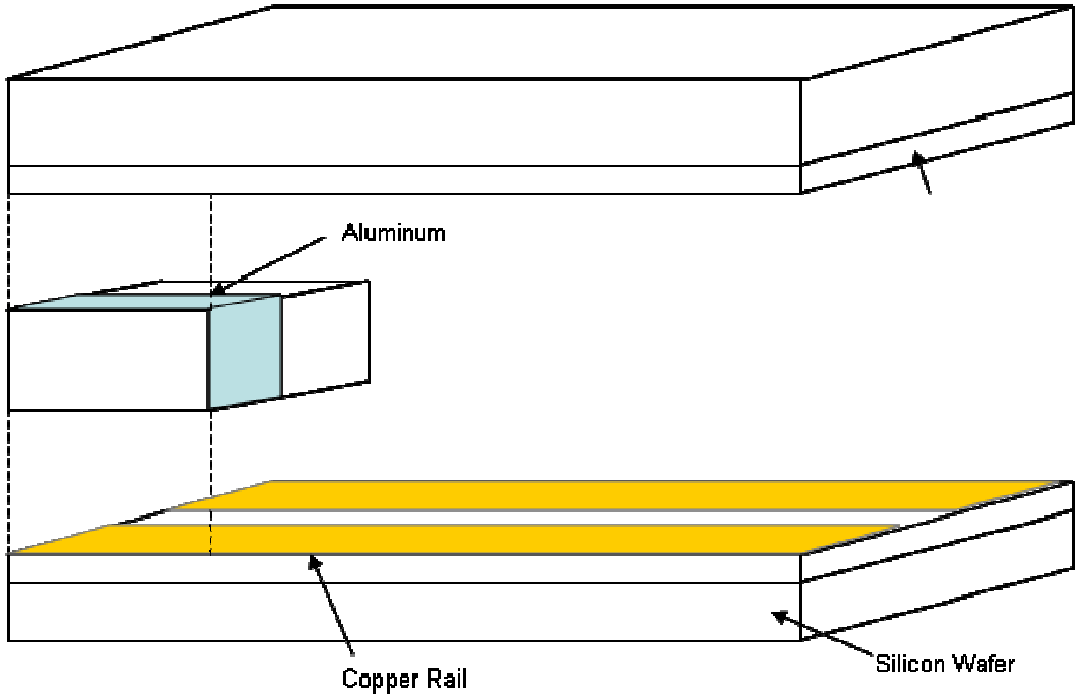

Figure 7. A schematic of the railgun static model setup. The Al 1100 foil was overlayed and pressed against the etched copper strips.

The Agilent E3632A power supply was connected to the test sample via the electrical feedthrough on the vacuum furnace end cap. Inside the furnace the feedthrough was connected to copper wires with high temperature insulation, which was rated to an operating temperature of 450^{o} C. Final operating temperatures at the middle of the

furnace would exceed the allowable 450^{o} C capacity of the insulated wires. To alleviate the concern of scorching the insulation and damaging the samples the wires were cut before reaching the heated zone and attached to bare copper wires. To prevent the copper wires from touching high temperature ceramic thermocouple insulators were used to insulate the wire. These insulators were rated to 1950^{o} C and were rated for use in vacuum.

The ends of the copper wires were affixed to pure copper alligator clips with smooth clamps to prevent damage to the test sample and maximize contact area. The clamping power of the spring inside the alligator clip became reduced at the high temperatures it was subjected to. To help maintain the clamping power screws were placed in the alligator clips to reinforce the clamps.

3. Test Procedure

Once the test specimen was assembled it was placed inside the vacuum furnace. The system was washed thoroughly with the Ar/H_2 gas and then sealed. The vacuum system was activated and time was given for the vacuum pressure to stabilize. Vacuum pressures would stabilize at approximately $4x10^{-4}$ torr in about 15 minutes. Once a stable vacuum was achieved the furnace was heated at 10^{o} C per minute so as to not thermally shock any components. The furnace was set to 500^{o} C which resulted in a measured internal tube temperature of 475^{o} C. Once the temperature had stabilized the power was applied, as depicted in Figure 8, and data recording of the voltage and current was started.

A constant DC current of 4Amperes was applied to the test sample for a predetermined duration and the associated voltage was measured as a function of time. At the end of the experiment, the power was removed and furnace was turned off. Once the furnace had cooled sufficiently the vacuum pressure was relieved and test sample was removed for analysis.

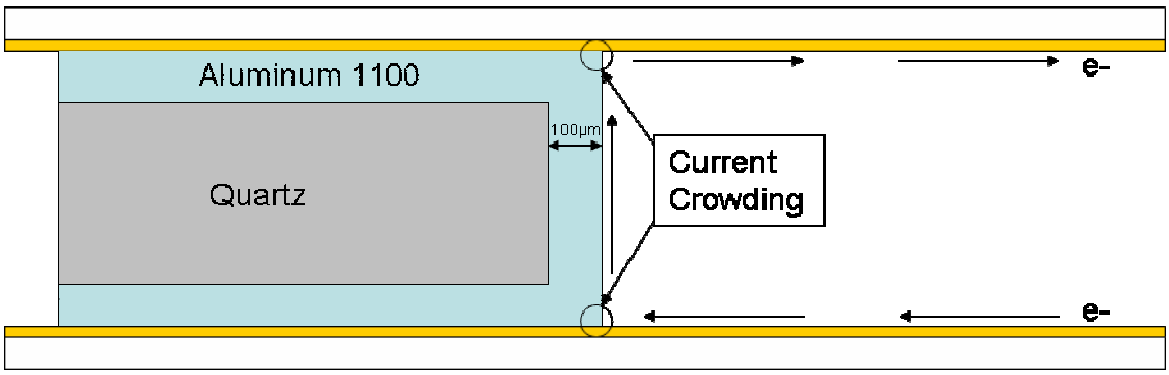

Figure 8. Schematic of Test Sample with Power Applied

4. Characterization Methods (Optical, SEM, EDS)

Following the completion of the experiment, initial observations of the test sample were conducted optically. Obvious damage to the armature and rails was noted and any evidence of oxidation of the rails and copper wires was searched for. The sample was then observed under the stereomicroscope for further examination before being disassembled. The samples were photographed and labeled.

The next step in analysis came from observations in the Scanning Electron Microscope (SEM). The SEM allowed high magnification pictures to be taken and had good contrast in topography of the sample. In addition to the topographical observations, the microstructure was also observed in the SEM.

Further analysis was conducted using the Energy Dispersive Spectrometer (EDS); in order quantify the composition percentage of each element at specific points to understand the interaction of the metals in the system.

V. RESULTS AND DISCUSSION

A. TEST RESULTS

Four tests were conducted with an initial internal tube temperature of 475^{o} C and an applied current of 4 amperes. The dimensions of the armature with a thickness of 76 microns and the copper rail width of 1mm gave a cross sectional area of 7.62×10^{-4} cm^2. This gave a current density through the armature of 5.25×10^3 A/cm^2. This current density matched well with other railgun experiments which achieved current densities of 4.8×10^3 A/cm^2 in the skin layer. The current density was at the low end of the spectrum and significant electromigration by "electron wind" forces was not likely. The tests were conducted four different times: (1) 60 hours, (2) one hour, (3) 15 minutes and (4) two minutes. Since the furnace was sealed and there were no viewports it was not possible to see any visual changes to the test sample while the test was being conducted. The only observations which could be made during the test were the in situ changes in voltage. The voltmeter was programmed with the computer to record every 30 seconds for the 60-hour, one-hour and 15-minute test. For the two-minute test, measurements were recorded every second.

1. 60-Hour Test

The first test was conducted for a duration of 60 hours. This test sample had the aluminum foil covering the entire width of the substrate. This was a practice that was modified in later tests. The initial temperature of the tube furnace was 475^{o} C and the current was set to 4 amperes. The voltmeter recorded a large jump in the voltage at the beginning of the test reaching a peak of 7.54 volts before falling to a low point of 3.57 volts about 30 minutes in to the test. From that point the voltage oscillated, but increased steadily until the end of the test where a voltage of 7.72 volts was recorded at 65 hours as shown in Figure 9. After this point the contact was lost and the data recording stopped. It was observed that the alligator clip springs became weakened due to the heat treatment and failed.

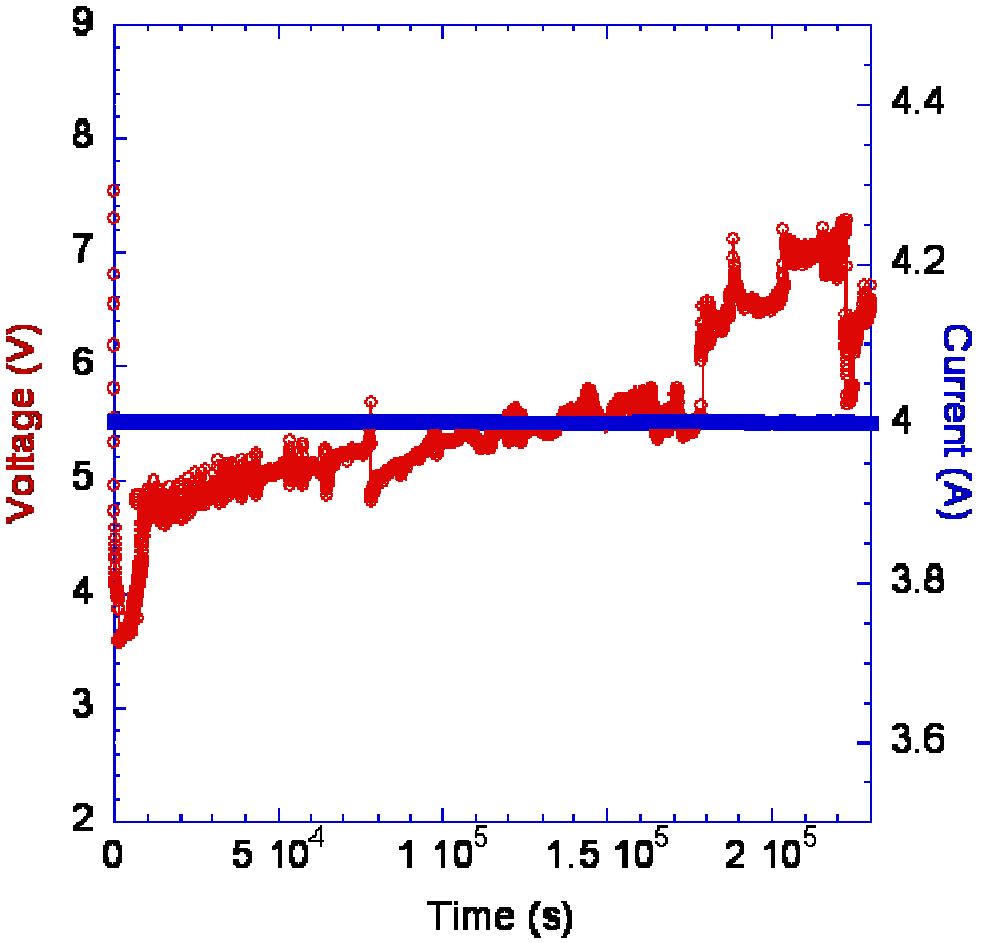

Figure 9. Voltage and Current vs. Time for 60-hr test

Observation of the sample once removed from the furnace revealed that the aluminum armature had been severely damaged and fused with the copper rails and silicon substrate. Also observed was a flow of aluminum along the rail towards the negative terminal, see Figure 10. The flow of molten aluminum was confined to the copper rail and was not spread over the entire substrate, an indication that electromigration had likely occurred. It was also observed that the aluminum fused with the substrate of the entire contact area and not just where the current passed through. The fusing was due to the joule heating which must have raised the temperature of the sample to at least the solidus temperature of aluminum alloy.

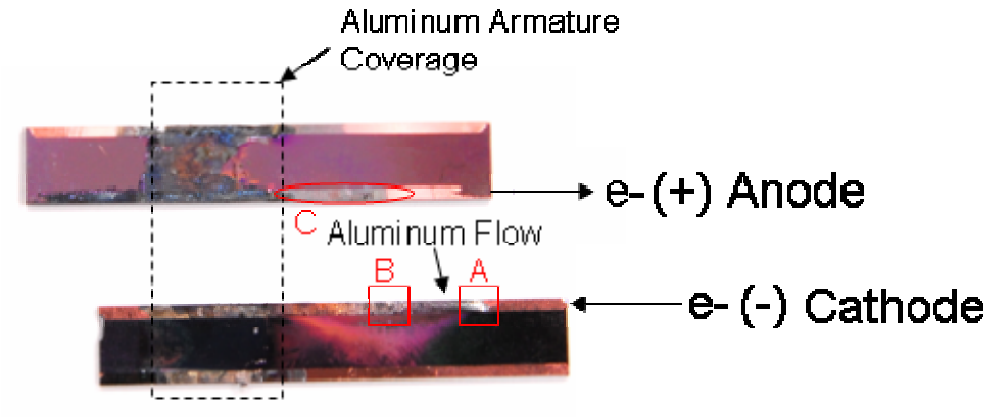

Figure 10. Rail Damage and aluminum Flow for 60-hr test

The sample was place in the SEM for observation of the microstructure. Observations were made of the sample along the rail from the armature to the alligator clip at the negative terminal. It was observed that the aluminum had piled up significantly in the vicinity of the alligator clip at the cathode which indicates that the aluminum had moved to that region quickly and continued to flow resulting in a pile up. Analysis of the microstructure at the end of the flow (Region A in Figure 10) showed predominantly aluminum microstructure with little alloying, see Figure 11.

In the region of the rail closer to the armature the layer of aluminum was much thinner and was alloyed with the copper from the rail, see Figure 12. This can be attributed to the longer duration in which this region had aluminum and copper in contact. It is also attributed to the fact that as the bulk of the aluminum moves along the rail it leaves only a thin coating of aluminum behind which can more easily mix with the copper from the rail. In the two-phase microstructure of Figure 12 (Region B in Figure 10), EDS analysis shows that the light area (Region 1) consists of both aluminum and copper (probably $CuAl_2$), see Figure 13, and that the dark area (Region 2) is primarily aluminum (α-solid solution), see Figure 14.

Another observation was the removal of the copper from the rail on the anode side of the test sample (Region C). This may likely have been the result of the thin layer of copper being subjected to surface electromigration and moving towards the armature.

Figure 11. Aluminum pile under the alligator clip in region A of test sample.

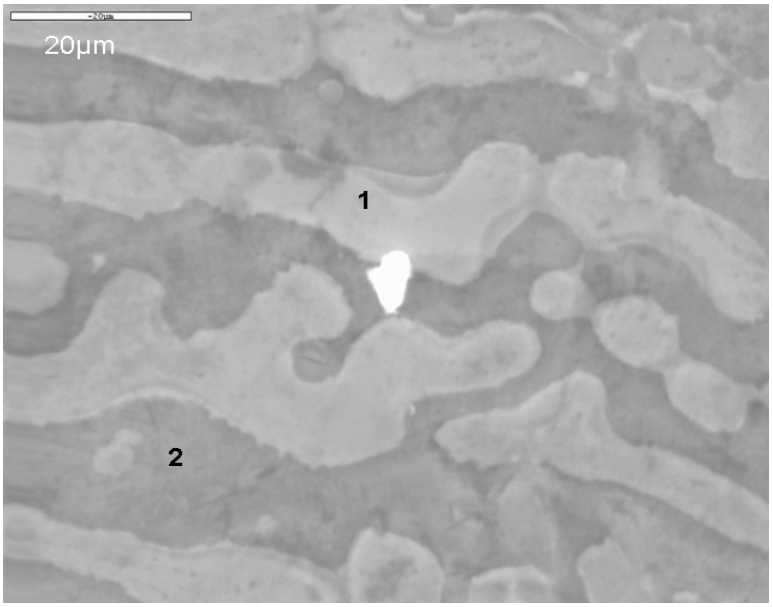

Figure 12. SEM Micrograph of the two-phase Al/Cu microstructure (Region B) between the Armature and Alligator Clip on the Cathode side rail. The Dark Regions were mostly pure Aluminum. Light Regions were well alloyed Al/Cu.

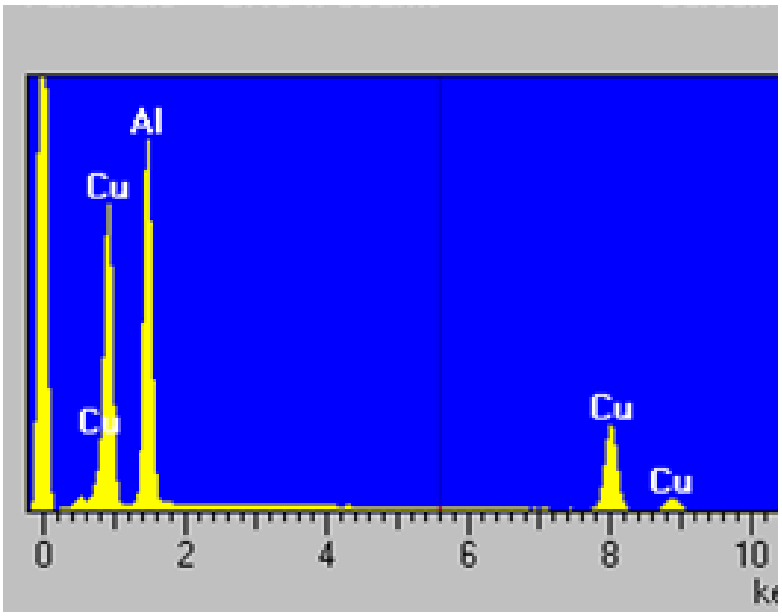

Figure 13. EDS Analysis of light area (Region 1) in Figure 12. Results show well alloyed Copper and Aluminum.

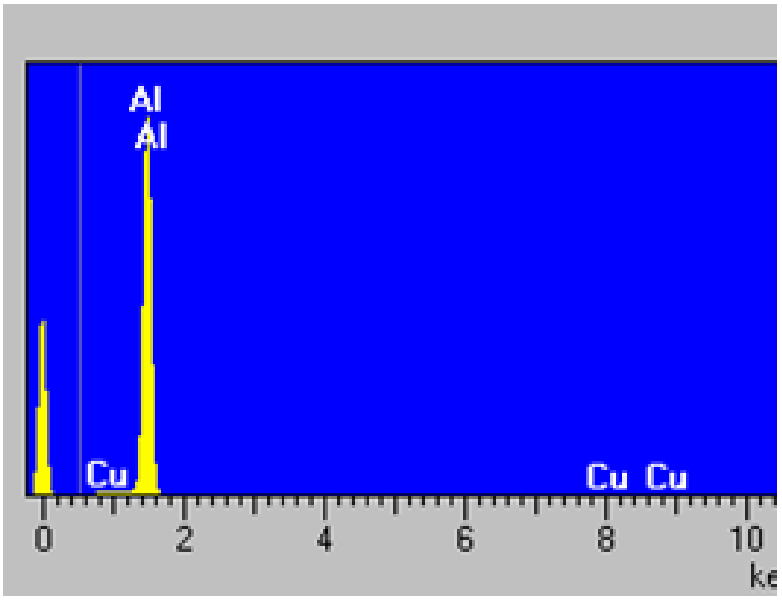

Figure 14. EDS Analysis of dark area (Region 2) in Figure 12. Results show the region is mostly pure Aluminum.

2. One-Hour Test

Based on the massive aluminum transport seen during the 60-hour test a second test was conducted for only one hour. The goal was to conduct the test for a duration that would show less significant damage and transport than was observed in the 60-hour test. Another modification was to reduce the width of the aluminum foil strip to be just

slightly wider than the copper rail. The intention of reducing the foil width was to maximize the current density through the aluminum armature and to observe the secondary copper rail when not in contact with the armature.

Test parameters were carefully noted for this test. Initial tube temperature was 475^{o} C. The vacuum pressure was $3x10^{-4}$ torr and current was set to maintain 4 amperes.

The results of this test confirmed what was seen in the previous test and provided further insight in to the reactions seen previously. As shown in Figure 15, significant aluminum transport was observed towards the cathode. The aluminum from the armature that was in contact with the rail was fused and badly damaged, and the copper rail in contact with the aluminum was severely damaged, possibly because of arcing as well as alloying with liquid aluminum. The copper rail that was not in contact with the aluminum showed minor discoloration; the cause of this damage is unclear.

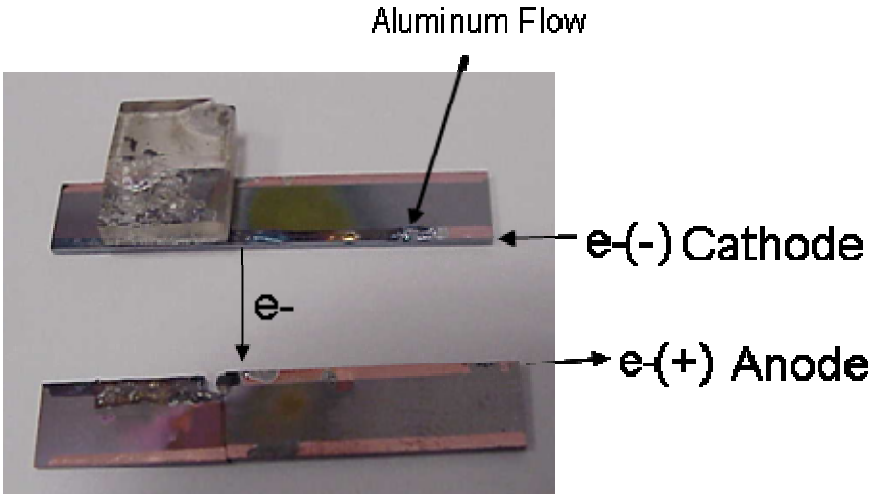

Figure 15. Test Sample after one-hour test. Less damage was observed to the copper on the anode side. Significant aluminum transport was still observed towards cathode.

The sample was observed in the SEM to characterize the microstructure and compare it with the previous test. It was observed that although the aluminum was transported all the way to the alligator clip at the cathode end of the rail the layer was thinner than on the 60-hour sample and a smaller pile was observed at the clip. Several

areas, outlined in Figure 16, were further analyzed with EDS to assess the composition. Also observed were cracks in the metal coating on the rail near the cathode end (Region A in Figure 16) as shown in Figure 17. The cracks appear to be the result thermal stress on the metal as it was cooled.

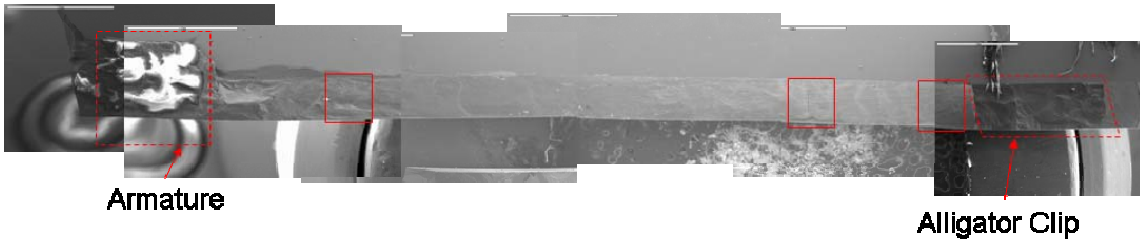

Figure 16. Montage of SEM micrographs of the cathode rail from the one-hour test. Solid outlined areas indicate further analysis was conducted with EDS.

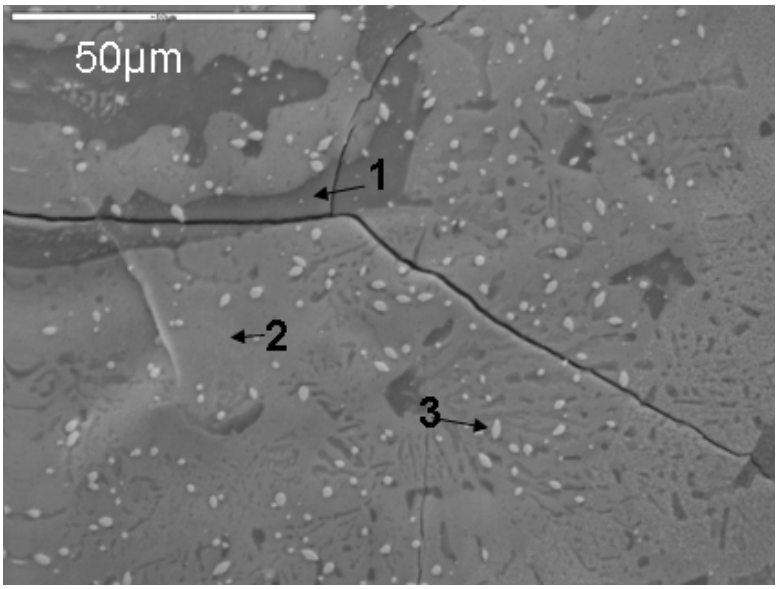

Figure 17. SEM observation of the one-hour test sample (Region A in Figure 16). Sample shows significant alloying, but also damage from cracking.

EDS analysis of the rail in the region next to the cathode alligator clip showed well alloyed copper and aluminum on the rail. The region showed an alloy similar to that observed in the middle of the rail in the 60-hour test. The dark area (Region 1 in Figure 17) was analyzed with EDS to be primarily silicon shown in Figure 18. This finding indicates that the copper coating has been moved in these regions by some form of transportation and that the coating in the surrounding area must be thin. The removal of the copper is likely due to the alloying with the aluminum in the surrounding area. The

thin nature of the surrounding area indicates that shorter duration of this test prevented a massive pile up of aluminum at the cathode terminal.

The gray area (Region 2 in Figure 17) was analyzed with EDS and was determined to be the well alloyed region of copper and aluminum. It was calculated that copper made up 46.21% of the composition and aluminum made up 41.67% of the composition, seen in Figure 19. The white dots (Region 3 in Figure 17) were also analyzed and the composition was found to be primarily tantalum nitride at 55.52% of the composition. The other large component of these areas was silicon at 22.07%, followed by copper at 9.47% and aluminum at 7.05%, see Figure 20. It appears these white dots are the consolidation tantalum nitride mixed with minor traces of copper and aluminum. The silicon detected by EDS is possibly attributed to the thinness of the layer, indicating that most of the copper has moved away from this region, and the penetration of the EDS beam in to the substrate.

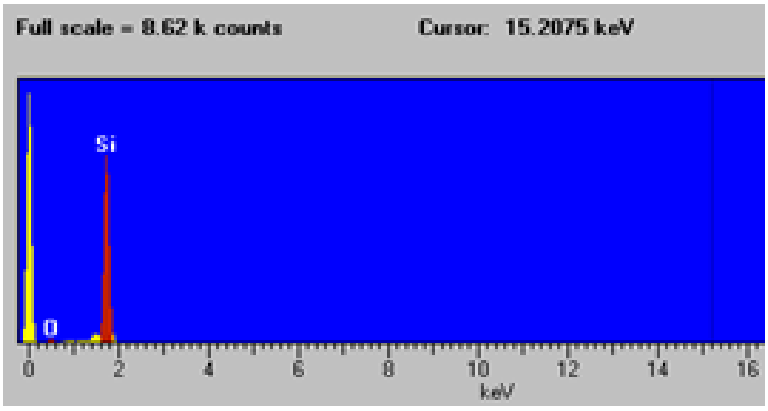

Figure 18. EDS analysis of the dark area (Region 1) seen in Figure 17. The region is completely Silicon (84.94%), 15.06% O, and indicates the removal of the copper coating. Also verifies the thinness of the metal covering the rail in surrounding area.

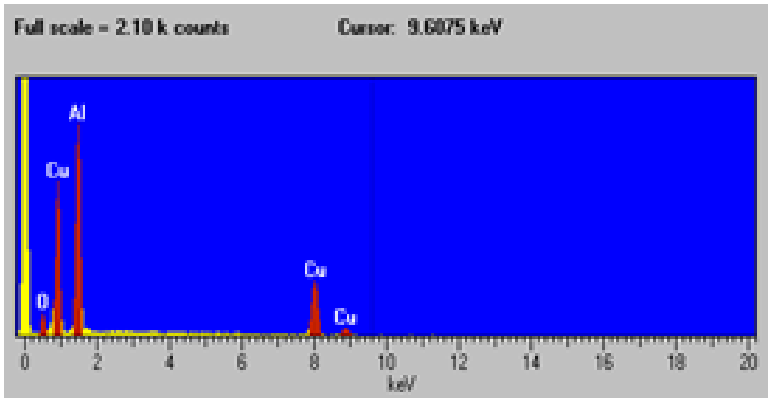

Figure 19. EDS analysis of the gray region (Region 2)seen in Figure 17. The region is a well alloyed containing 46.21% Copper and 41.67% Aluminum.

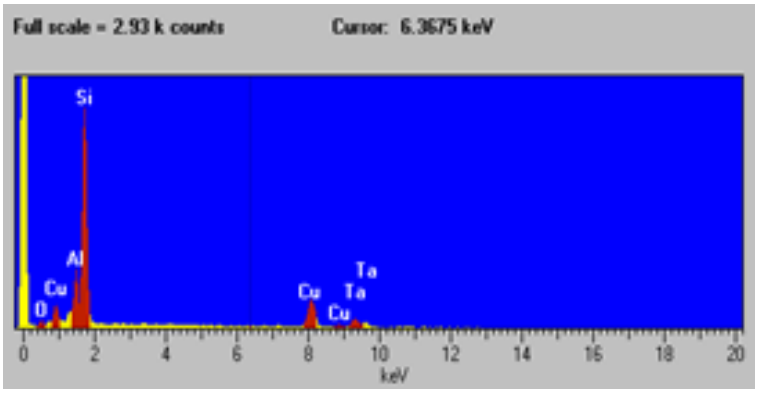

Figure 20. EDS analysis of the white dots (Region 3) seen in Figure 17. The region is primarily a consolidation of Tantalum Nitride (55.52%) on the Silicon (22.07%) substrate. Traces of Aluminum (7.05%) and Copper (9.47%) are mixed in to these areas.

The region in the middle area of Figure 16 (Region B) was analyzed further after seeing interesting cracking formations in the region, see Figure 21. Large area EDS analysis of two areas noted in Figure 21 was conducted. The overall outline of the original copper rail is seen in Figure 21 and a layer of alloy appears to be on top of the original layer. First EDS analysis was conducted on the bottom layer (Region 1) and it was surprisingly composed almost entirely of silicon, see Figure 22. This indicates that the copper from the rail in this region had been completely removed and transported.

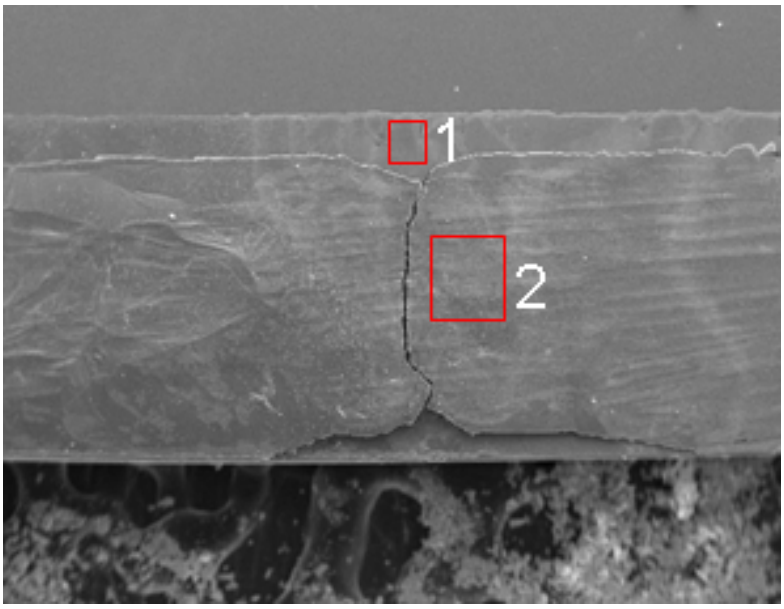

Figure 21. Middle area (Region B in Figure 16) of cathode rail region from one-hour test. Regions outlined in red were further analyzed with EDS.

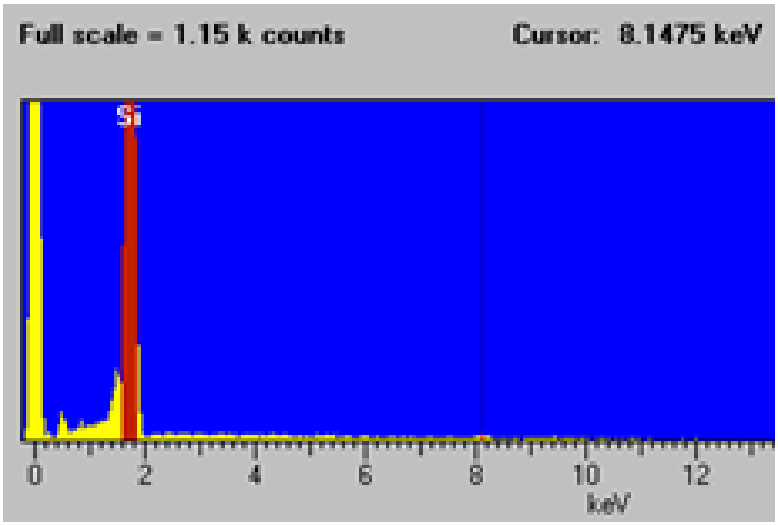

Figure 22. EDA analysis of bottom layer (Region 1) seen in Figure 21, indicated the smaller red boxed. The region is composed entirely of Silicon.

The second area of analysis from Figure 21, (Region 2), was the top layer that appeared to be a well alloyed microstructure, see Figure 23. The composition of this area was 54.22% aluminum and 21.67% copper, see Figure 24. This result again indicates that the aluminum and copper will diffuse in to each other and form an alloy.

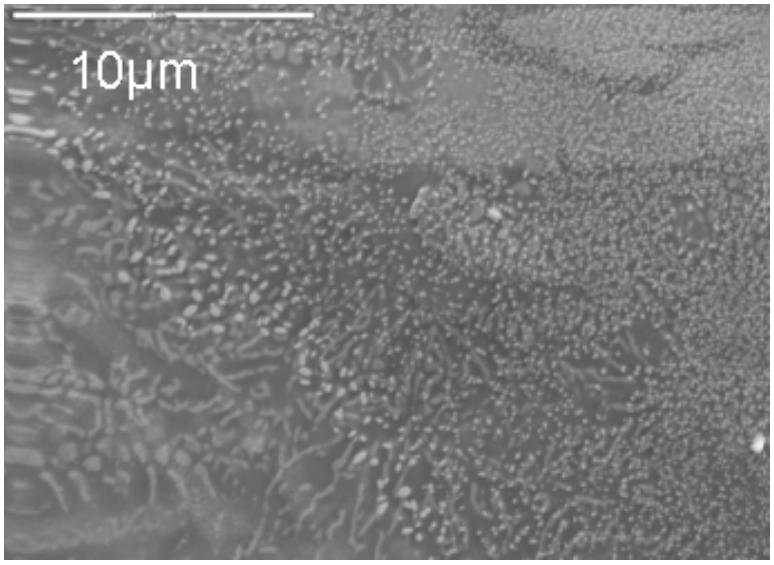

Figure 23. SEM micrograph of top layer (Region 2) seen in Figure 21.

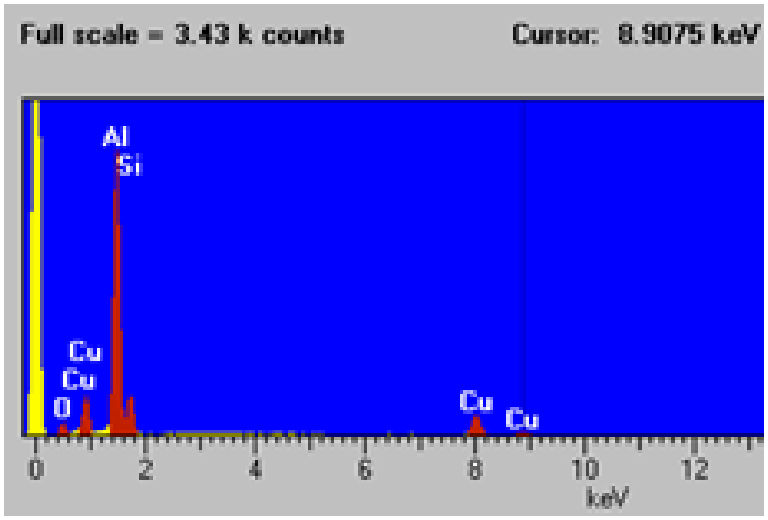

Figure 24. EDS analysis of the top layer (Region 2) seen in Figure 20. The region is an alloy containing 54.22% Aluminum and 21.67%% Copper.

The final area that was examined on this test sample was in the region close to the armature on the cathode rail (Region C), indicated in Figure 16. This region would have had the largest amount of aluminum flow over it and had the longest time period to alloy with copper from the rail. The microstructure appears similar to that seen in the middle of the rail; see Figure 25, indicating that the aluminum flowed over the rail in bulk leaving a consistent residual thickness on the rail. The amount that remained is what alloyed with the copper from the rail. EDS analysis was conducted on both the dark and light areas

seen in Figure 25 to determine its composition. The dark area (Region 1) was primarily aluminum with 87.13% of the composition and copper consisting of just 9.72%, see Figure 26. The light area (Region 2) however, was well alloyed consisting of 48.04% copper and 42.07% aluminum, see Figure 27.

Figure 28 shows a plot of the voltage and current measured in the circuit during the test. Similar to what was seen in the 60-hour test, see Figure 9, the voltage peaks initially and the drops steadily for several minutes at the beginning of the test. Upon reaching a low point the voltage slowly increases, indicating an increase in resistance, until the test was terminated. Again, it appears that contact resistance is responsible for the initial voltage spike. Melting and fusing of the armature and rails improves contact and reduces resistance resulting in a drop in voltage until equilibrium is reached. Finally, the electromigration and alloying effects begin to take effect and resistance increases for the remainder of the test.

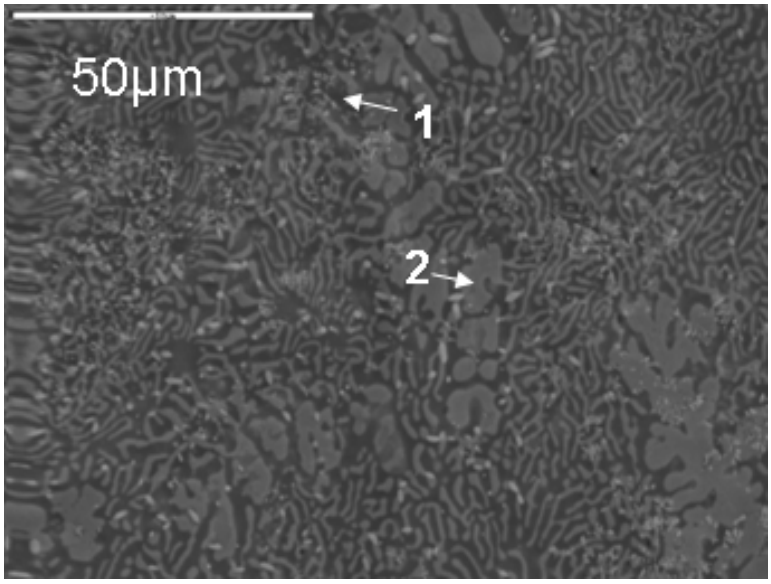

Figure 25. SEM micrograph of area (Region C) in close proximity to the armature on the cathode rail.

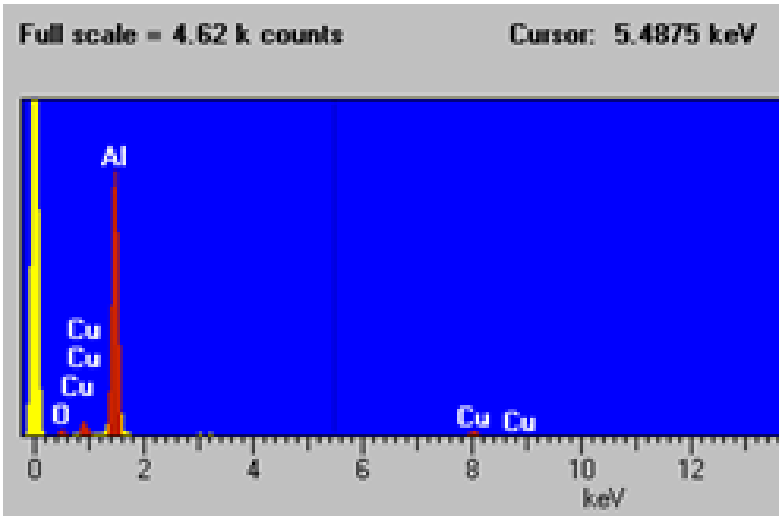

Figure 26. EDS analysis of the dark area (Region 1) seen in Figure 25.

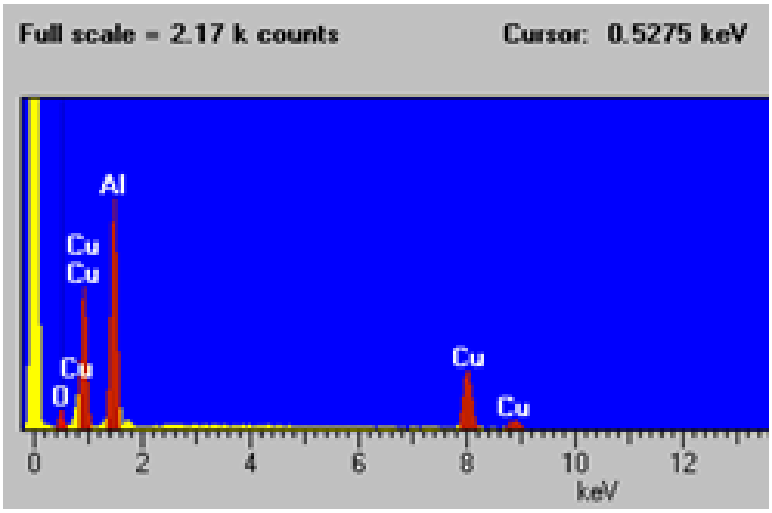

Figure 27. EDS analysis of the light area (Region 2) seen in Figure 25. The region is an alloy containing 42.07% Aluminum and 48.04%% Copper.

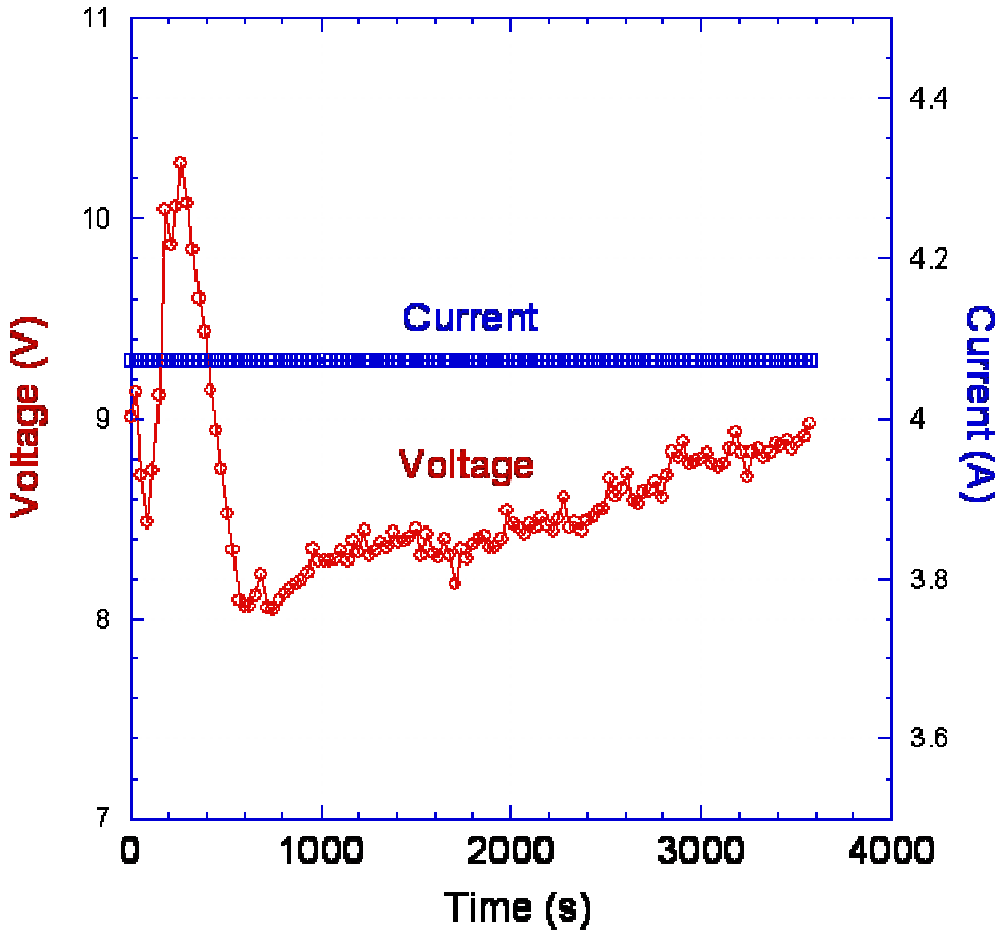

Figure 28. Voltage and Current versus time for one-hour test.

3. 15-Minute Test

The third test conducted was for a duration of 15 minutes. This was done in an attempt to further reduce the amount of metal transport and alloying of copper and aluminum. The parameters for the test were the same as the one-hour test. The furnace was set to an initial internal temperature of 475^{o} C, the vacuum pressure was 3x10^{-4} torr and 4 amperes of current were run through the sample. Again the aluminum foil was cut so as to not cover the entire substrate and thus leave the secondary rail untouched.

In Figure 29 the aluminum flow, as seen in the previous tests, is present. Also observed was a cooled molten ball of aluminum on the anode rail and in contact with the armature. Observation of this region reveals that the aluminum appears to have melted

due to Joule heating and flowed on to the anode rail due to gravity. It is expected that this metal would have been transported to the cathode side given adequate time with current applied. It was also observed that the rails that were not in contact with the aluminum suffered no damage confirming that the Joule heating of the sample was not elevating the sample to the melting point of copper.

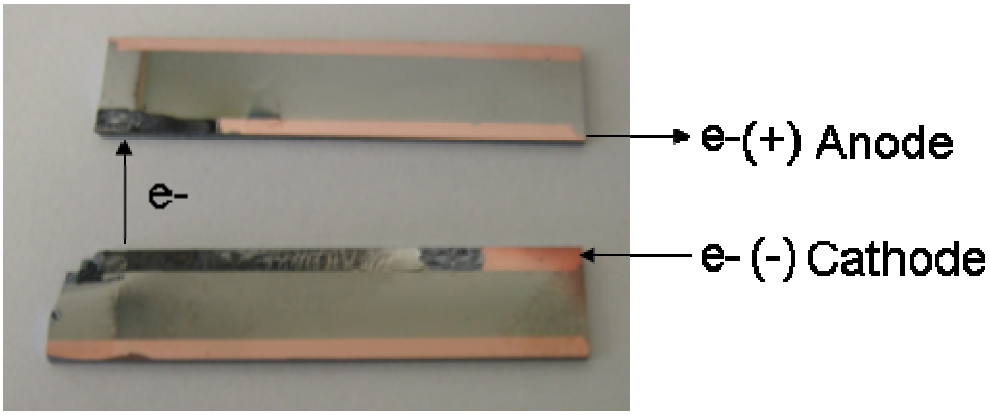

Figure 29. The 15 minute test sample showing the flow of aluminum along the cathode rail. Melted aluminum in on the anode rail in a molten ball, but does not appear to have been transported.

The rails from third test were placed in the SEM for observation. Two areas were evaluated with EDS for composition analysis. These areas are outlined in red boxes in Figure 30 and are similar in relative position as the regions analyzed in the one- hour test.

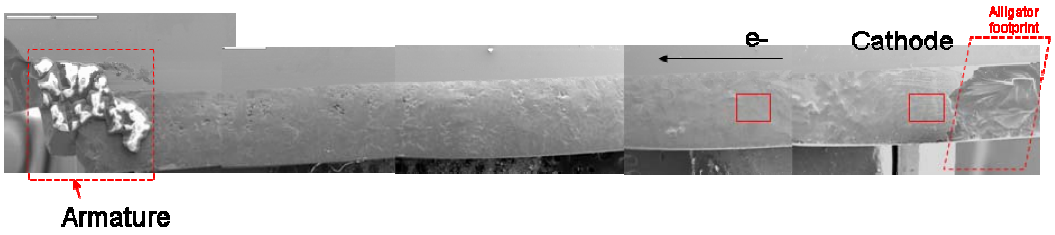

Figure 30. SEM micrograph of the cathode rail from the 15 minute test. Solid outlined areas indicate further analysis was conducted with EDS.

The area closest to the alligator clip (Region A in Figure 30) on the cathode rail would have the least time exposure to the aluminum since it is the furthest area from the armature and this was the shortest test. It was observed that the aluminum was still

transported across the entire rail in the short time period. The microstructure, however, was different than seen previously, see Figure 31. The microstructure had a feather, or frostlike, appearance which indicated that perhaps this section was not well alloyed yet. EDS analysis was conducted on the region and the dark areas (Region 1 in Figure 31) were observed to be predominately silicon, composing 94.56% of the area, see Figure 32. The light areas (Region 2 in Figure 31) were composed of 53.52% copper and 42.78% aluminum indicating the area is well alloyed, see Figure 33. The combination of these observations indicates that the copper coating on the silicon was transported and mixed with the aluminum in the alloy regions. Observation of Figure 31 shows that the conducting alloy is broken and does not present a clean path for the current to flow. This is a likely cause of increasing resistivity of the rail and results in the rise in voltage, see Figure 34, needed to supply the steady 4 amperes programmed in to the power supply.

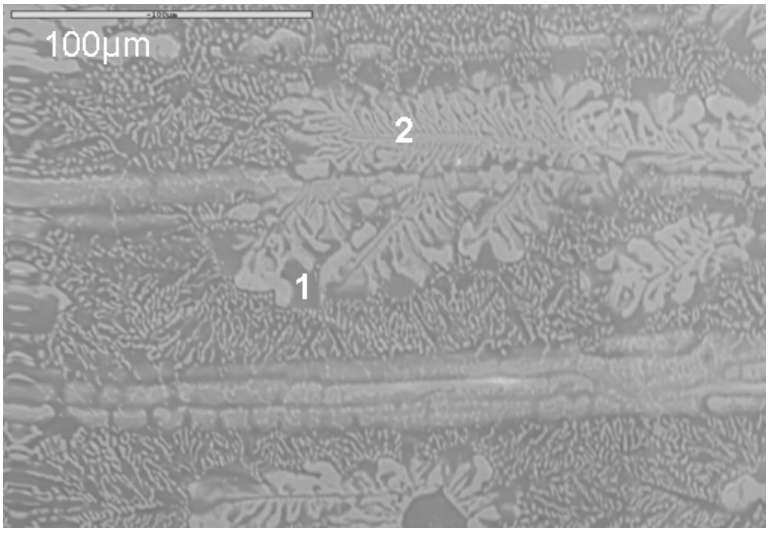

Figure 31. SEM micrograph of the cathode rail section near the alligator clip. New lines and featherlike microstructure seen here.

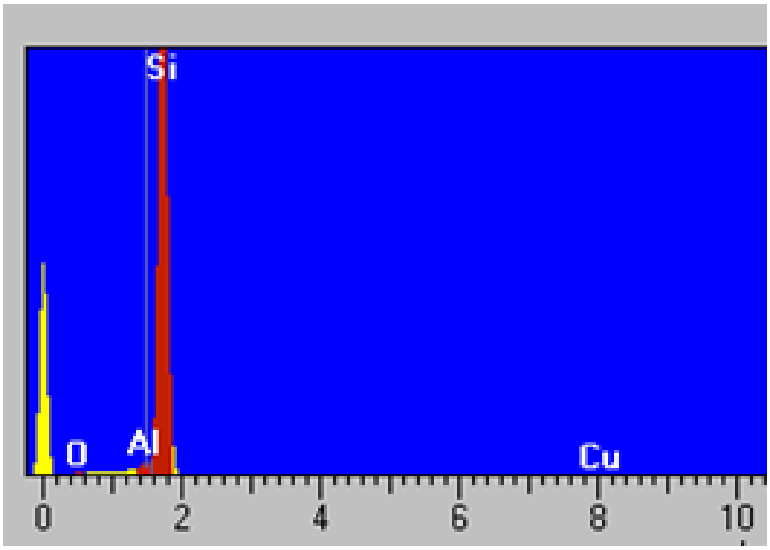

Figure 32. EDS analysis of the dark area (Region 1) in Figure 31 on the cathode rail near the alligator clip. The region is predominantly Silicon.

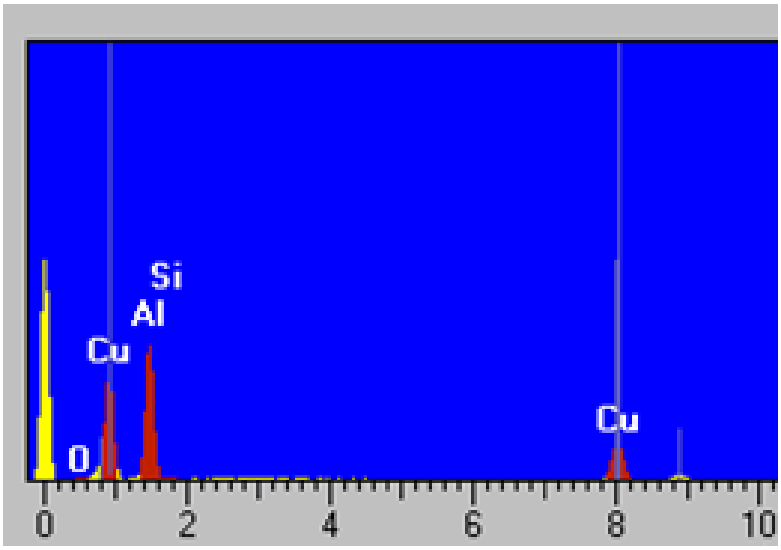

Figure 33. EDS analysis of the light area (Region 2) in Figure 31 on the cathode rail near the alligator clip. The region is an alloy containing 42.78% Aluminum and 53.52%% Copper.

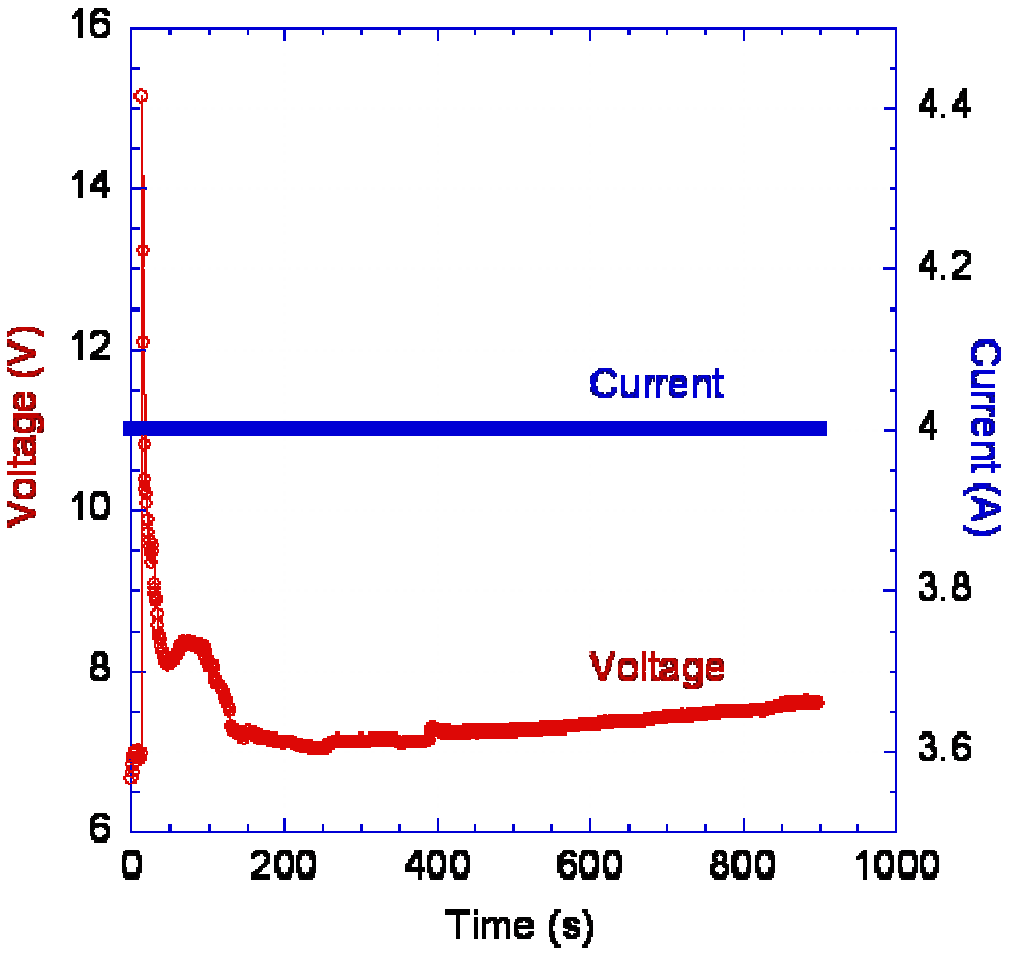

Figure 34. Voltage and Current versus time for 15 minute test.

4. Two-Minute Test

The final test was conducted for a period of 130 seconds. The duration of this test was not predetermined; instead it was determined by watching the value of the voltage during the test. The voltage peak was observed and the test was allowed to continue until the low point of voltage was reached. Once the voltage began to increase the test was terminated, see Figure 35.

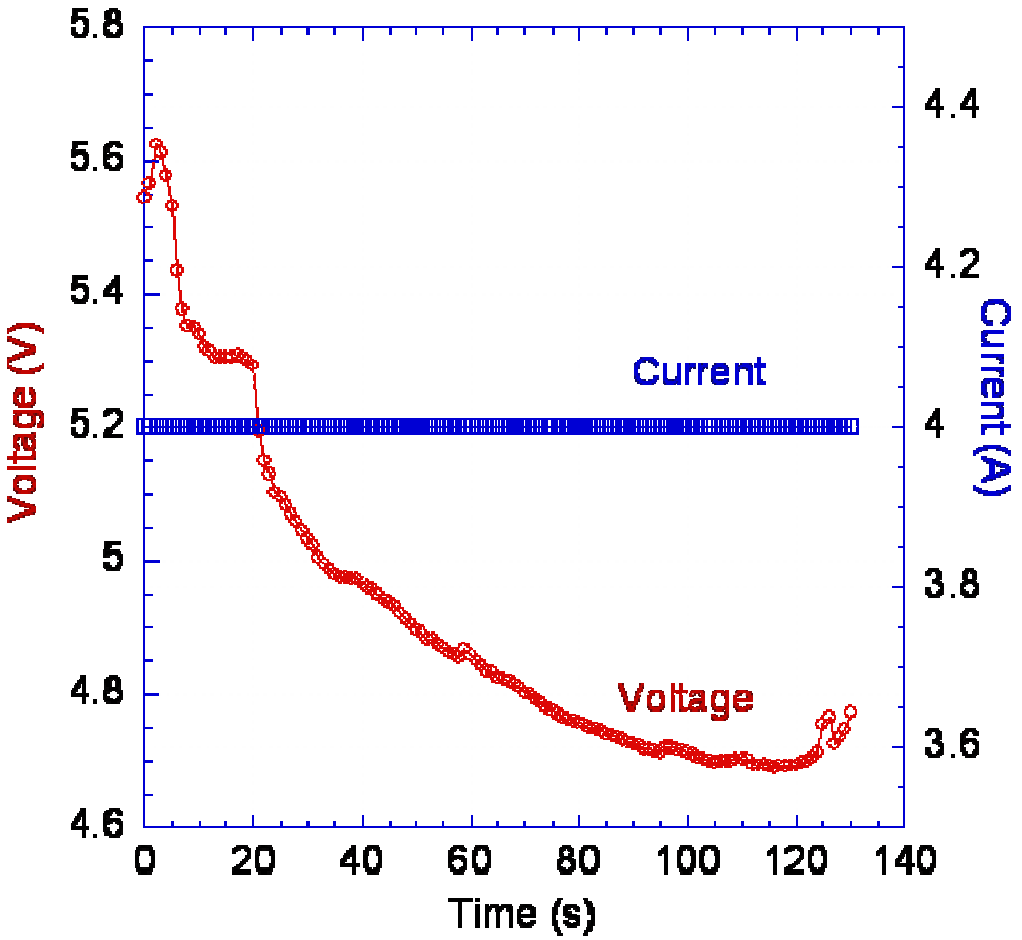

Figure 35. Voltage and Current versus time for two minute test.

The two minute test proved to be very successful and showed results not observed in the previous tests. The primary difference for this test was that the electromigration transport of the aluminum did not reach the alligator clip on the cathode terminal. This allowed measurement of the actual distance the aluminum covered during the test, see Figure 36. The measured distance of aluminum coverage was 5.14 mm. This meant that on average the aluminum movement was approximately 0.039 mm/sec.

Also observed from this test were the characteristics of the aluminum at the early stages of melting and movement. Unlike previous test the aluminum of the armature retained its shiny luster appearance. Previously that aluminum had been blacked and brittle, possibly due to a reaction with silicon from the substrate. The condition of the aluminum allowed closer observation of the armature bridge between the two rails. The

thickness of the bridge was measured at approximately 400 microns. This meant that the thickness of the bridge increased during the duration of the test. This increase must have resulted from the movement of molten aluminum from the region compressed between the rail and quartz to the bridge.

Analysis of the microstructure from this test sample also showed new characteristics. The characteristics of the metal at the leading edge region of the flow were significantly different from what had been seen before. Figure 37 shows the large gray areas (Region 1) that form at the lead of the flow. EDS analysis shows the composition of the large gray areas of this flow to be 59.17% aluminum and 40.83% copper, see Figure 38. The areas (Region 2) in between the large gray areas were similar in microstructure to the well alloyed areas seen in previous tests. It can be concluded that the large gray areas are in the initial stages of the alloying process and are largely a coating of aluminum covering the copper rail.

Figure 39 shows the microstucture of the cathode rail near the armature. It has already become a well developed alloy in less than two minutes. There are also some feather-like characteristics in the figure which are similar to those seen near the cathode alligator clip in Figure 31 during the 15 minute test. The feather-like characteristics are not present in the other test which represents that this is also a transitory characteristic of the microstructure which is not fully developed like those seen in Figure 23 and 25.

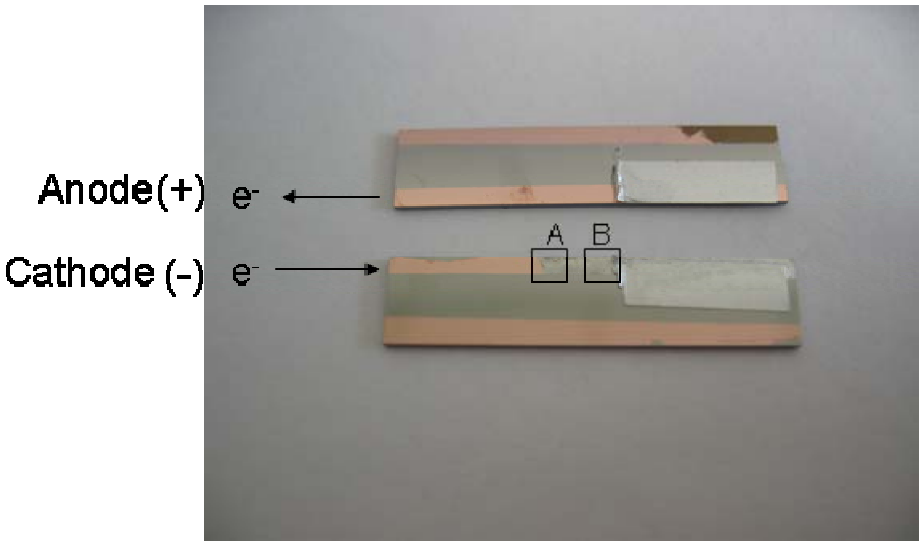

Figure 36. The two-minute test sample showing the flow of aluminum along the cathode rail. The aluminum of the armature has melted and fused with the substrate, but is largely undamaged.

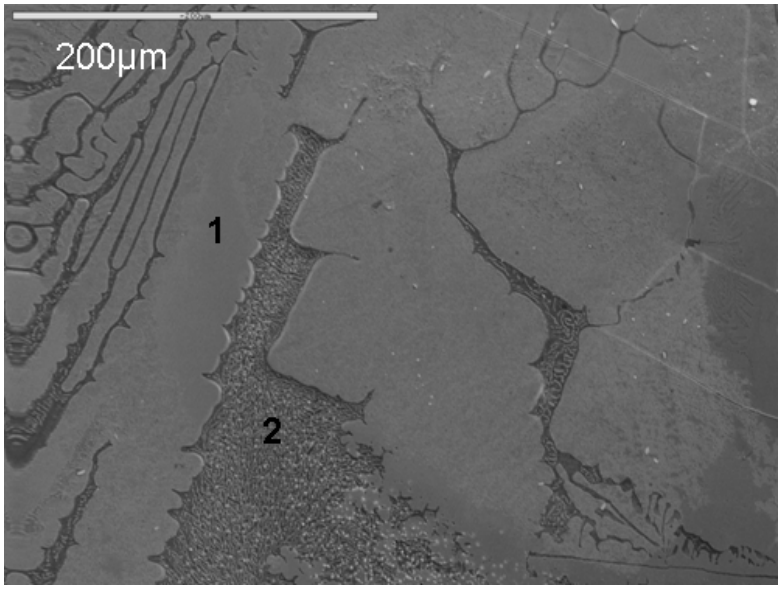

Figure 37. SEM Micrograph of the leading edge of the flow (Region A in Figure 36) on the cathode rail.

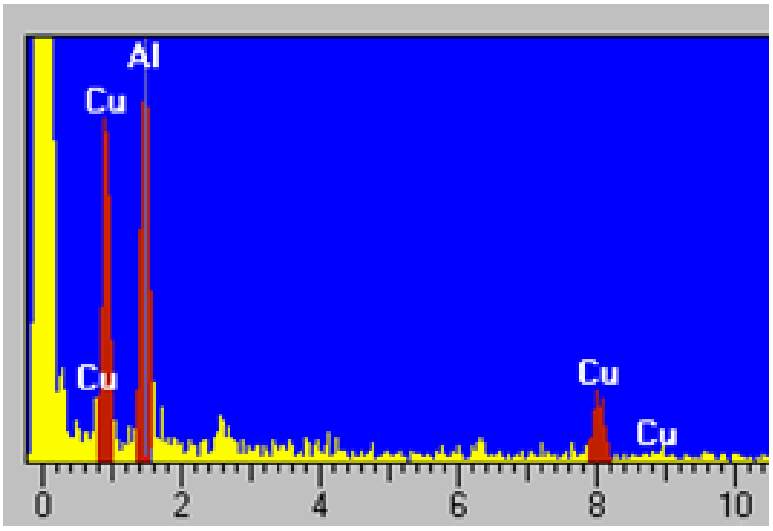

Figure 38. EDS analysis of the large gray areas (Rregion 1) seen in Figure 37. Analysis shows the region is 59.17% Aluminum and 40.83% Copper.

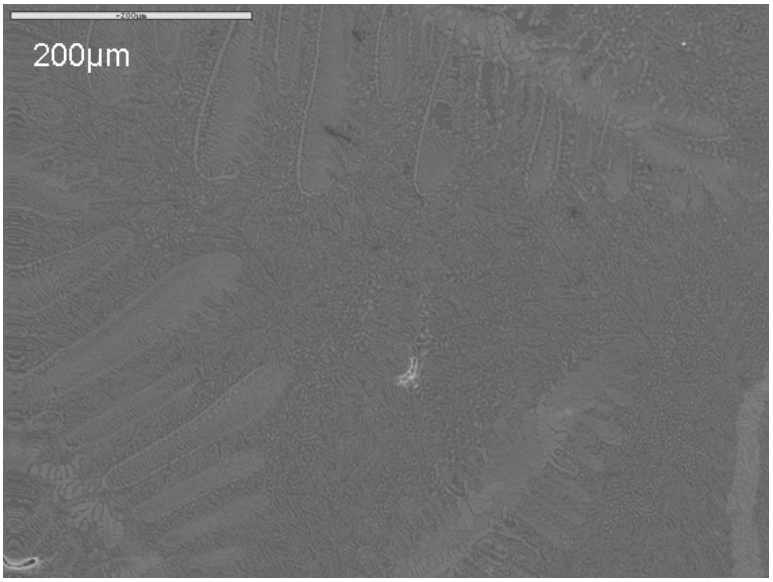

Figure 39. SEM micrograph of the rail in the two-minute test near the armature. The sample has already become a well developed alloy.

B. DISCUSSION OF METAL FLOW AND MICROSTRUCTURE

The flow of aluminum was much more significant and much quicker than originally expected. Based on the background study of surface and liquid metal electromigration a mass transport of aluminum towards the cathode would be expected at the low current density and high temperatures in these tests. However, the result was more dramatic than expected. The Joule heating from the applied current raised the temperature of the test sample above the melting point of aluminum almost

instantaneously. This is most likely due to the high contact resistance of the copper-aluminum interface. The molten aluminum then quickly began migrating along the cathode rail in the direction of the current flow.

The rate of flow was so much larger than expected that it was not until the two minute test that the flow was stopped before reaching the alligator clip at the cathode terminal. Being able to analyze the leading edge of the flow was crucial to understanding the development of alloying observed in all the samples. Figure 37 shows that even at the leading edge of the flow, alloying between copper and aluminum, which was observed after large durations in the other tests, were already starting to form. The microstructure development includes the formation of feather-like formations, see Figure 39, and then the fully developed alloy, see Figure 25.

The rapid transport and alloy development of the test samples seen in this testing has serious implications if they carry over to the full scale railgun. The degradation of the armature is significant and begins almost instantaneously. The melting point of aluminum is quickly reached once current is applied and the transport of molten aluminum begins immediately. The degradation of the armature causes increased resistance, poor performance and severe damage to the copper rails.

The alloying of aluminum with the copper has not been studied in detail for full size railguns, except by Persad [33] who used aluminum rails and a copper armature in a laboratory railgun. In his research, Persad observed solidified droplets of $CuAl_2$ which had formed at the copper-aluminum interface. The molten droplets were then jetted out behind the armature as it moved along the rail. The characteristics of the newly formed $CuAl_2$ are that of an alloy which is harder and more resistive than pure metals. This alloy, which is similar to what has been seen in this study, will certainly cause severe wear on subsequent armature shots and will reduce the efficiency of the electrical circuit, resulting in poor performance of the projectile. Although other methods in which molten aluminum can form and come in contact with the copper rails has been discussed earlier, at least some of this alloying is quite likely due to the electromigration effects observed here.

C. DISCUSSION OF VOLTAGE AND CURRENT OBSERVATIONS

The current in the power supply was set to maintain 4 amperes for the duration of the experiments. This forced the power supply to alter the voltage level to maintain desired current. In all of the tests the voltage spiked upon initiation and then quickly decreased until a low point was reached. This indicates that resistance initially peaks and then decreases steadily for several minutes. The voltage then began a slow and steady increase until the test was terminated indicating an increasing resistance in the circuit. The resistivity is due to several factors; the interaction between the aluminum armature and copper rails, and the alloying of the copper and aluminum on the rails. Neither of these can be monitored directly during the experiment. However, several conclusions could be drawn about the resistance changes after observing the test samples upon removal from the furnace.

It appeared that the initial spike in voltage was caused by the arcing and high contact resistance between the armature and rails after test initiation. The high resistance in the test sample quickly raised the temperature of the sample via Joule heating and the aluminum began to melt. Once the melting occurred the molten aluminum provided intimate contact with the copper rails, decreasing the contact resistance between the two pieces. Also, as aluminum from the long "mounting" sections of the armature melted they were forced out by the pressure from the mounting clips. Some of this molten aluminum was forced on to the bridge joining the two rails. This increased the cross sectional area which decreased the resistance in the circuit. This process carried on until equilibrium was reached with the aluminum being transported along the rail via electromigration. At this point the aluminum supply became less than the amount being transported away and the resistance began to slowly increase again, as seen in all the voltage versus time figures.

Additionally once the aluminum came in to contact with the copper on the rails they began to form an alloy. The resistance of the copper/aluminum alloy is greater than that of pure copper and as the alloying increased the resistance increased as well. The alloying process also stripped the copper away from the substrate in some areas, see Figure 31 and 32. The removal of the copper decreased the direct path for the current to flow also increasing resistivity.

VI. CONCLUSIONS AND RECOMMENDATIONS

Observations of surface electromigration of liquid aluminum were made on a scaled down static railgun model developed for this study. The development of this experimental method for investigating damage of the aluminum armature due to electromigration was successful. The current in the armature reached a density of $5x10^3$ A/cm^2. The aluminum from the armature was found to quickly reach its melting point via Joule heating due to high contact resistance at the armature-rail contact. Once liquid aluminum was formed, it rapidly migrated along the copper rail towards the cathode (i.e. negative) terminal. Initial indications are that the molten aluminum flowed along the rail at a minimum velocity of 0.04 mm /sec at the applied current of 4 A.

Resistance in the circuit initially spikes due to arcing at the aluminum-copper contact after the current is applied. The melting of the aluminum reduces the contact resistance and the resistance of the circuit reduces for a short period. Once the aluminum begins to be transported along the rail towards the cathode terminal, it alloys with the copper and the resistance steadily increases in the circuit.

This transport of liquid aluminum along the copper rails was attributed to electromigration of the liquid under the influence of the direct electric field. This direction of electromigration of the liquid is opposite to the direction of conventional electromigration solids, where matter moves in the direction of electron flow under the influence of the electron wind force.

Testing for this study was conducted under vacuum. It is reasonable to expect that the environmental circumstances acting on the armature of an actual railgun will be much more severe. There were no dynamic contact pressure or friction forces that needed to be taken in to account in this test. Higher current density, dynamic contact resistance, friction and current crowding are to be expected on the full scale railgun. Therefore the possible effects of electromigration on the development of a sustainable railgun system require serious consideration.

Future study should be undertaken to further understand the kinetics of the liquid aluminum. The kinetics, once fully understood, can then be scaled to the size of current railgun prototypes to model damage potential. The damage on current railgun prototypes can be observed and correlated to the scaled damage seen in this study. If the results are matched, then electromigration is a significant challenge and steps can be taken to mitigate the problem.

LIST OF REFERENCES

1. Luke, I. T., M. F. Stumborg. "The Operational Value of Long Range Land Attack EM Guns to Future Naval Forces." IEEE Transactions of Magnetics 37.1 (2001) 58-61.

2. McNab, I. R. "Parameters for an Electromagnetic Naval Railgun." IEEE Transactions on Magnetics 37.1 (2001) 223-228.

3. Fair, H. D. "The Science and Technology of Electric Launch." IEEE Transactions on Magnetics 37.1 (2001) 25-32.

4. Weeks, D. A., W. F. Weldon. "Plasma-Armature Railgin Launcher Simulations." IEEE Transactions on Plasma Science 17.1 (1989) 403-408.

5. Thornhill, L. D. "Scaling Study for the Performance of Railgun Armatures." IEEE Transactions on Plasma Science 17.3 (1989) 409-421.

6. Wikipedia website, last accessed on 3 November 2006 http://en.wikipedia.org/wiki/Railgun

7. Barker, L. M., T. G. Trucano. "Railgun Rail Gouging by Hypervelocity Sliding Contact." IEEE Transactions on Magnetics 25.1 (1989) 83-87.

8. Stefani, F., J. V. Parker. "Experiments to Measure Gouging Threshold Velocity for Various Metals Against Copper." IEEE Transactions on Magnetics 35.1 (1999) 312-316.

9. Parks, P. B. "Current melt-wave model for transitioning solid armature." Journal of Applied Physics 67.7 (1990) 3511-3516.

10. Challita, A., J. P. Barber. "Railgun Armature Arcing Voltage Drop." IEEE Transactions on Magnetics 31.1 (1995) 118-122.

11. Stefani, F., R. Merrill. "Experiments to Measure Melt-Wave Erosion in Railgun Armatures." IEEE Transactions on Magnetics 39.1 (2003) 188-192.

12. Stefani, F., J. V. Parker. "Experiments to Measure Wear in Aluminum Armatures." IEEE Transactions on Magnetics 35.1 (1999) 100-106.

13. Satapathy, S., F. Stefani, A. Saenz. "Crack Tip Behavior Under Pulsed Electromagnetic Loading." IEEE Transactions on Magnetics 41.1 (2005) 226-230.

14. Chen, T., X. Long, I. Dutta, C. Persad. “Effect of Current Crowding on Microstructural Evolution at Rail-Armature Contacts in Railguns.” IEEE Transactions on Magnetics, in review, (2006).

15. Nearing, J. C., M. A. Huerta, “Skin and Heating Effects of Railgun Current.” IEEE Transactions on Magnetics 25.1 (1989) 381-386.

16. Long, G. C. “Railgun Current Density Distributions.” IEEE Transactions on Magnetics 22.6 (1986) 1597-1602.

17. Batteh, J. H., J. D. Powell, G. E. Rolader. “Effect of a Transient Current Profile on the Dynamics of Railgun Arcs.” IEEE Transactions on Magnetics 29.1 (1993) 739-744.

18. Ho, P. S., T. Kwok. “Electromigration in Metals.” Reports on the Progress in Physics 52 (1989) 301-348.

19. Blech, I. A. “Electromigration and crevice formation in thin metallic films.” Thin Film Solids 13 (1972) 117-129.

20. Blech, I. A., E. Kinsbron. “Electromigration in Thin Gold Films on Molybdenum Surfaces.” Thin Solid Films 25 (1975) 327-334.

21. Blech, I. A. “Electromigration in thin aluminum films on titanium nitride.” Journal of Applied Physics 47 (1976) 1203-1208.

22. Blech, I. A., C. Herring. “Stress generation by electromigration.” Applied Physics Letters 29.3 (1976) 131-133.

23. Black, J. R. “Electromigration- A Brief Survey and Some Recent Results.” IEEE Transactions on Electron Devices 16.4 (1969) 338-347.

24. Tu, K. N. “Recent advances on electromigration in very-large-scale-integration of interconnects.” Journal of Applied Physics 94.9 (2003) 5451-5473.

25. Lin, Y.H., Y. C. Hu, C. M. Tsai, C. R. Kao, K. N. Tu. “In situ observation of the void formation-and-propagation mechanism in solder joints under current-stressing.” Acta Materialia 53 (2005) 2029-2035.

26. Anthony, T. R. “The electromigration of liquid metal inclusions in Si.” Journal of Applied Physics 51 (1980) 6356-6365.

27. Epstein, S. G., A. Paskin. “Atom Motion in Liquid Alloys in the Presence of an Electric Field.” Physics Letters 24A.6 (1967) 309-310.

28. Regan, B. C., S. Aloni, R. O. Ritchie, U. Dahmen, A. Zetti. “Carbon nanotubes as nanoscale mass conveyors.” Nature 428.6986 (2004).

29. Yasunaga, H., A Natori. “Electromigration on semiconductor surfaces.” Surface Science Reports 15 (1992) 205-280.

30. Lodder, A. “Clarification of the Direct-Force Controversy in Electromigration Theory.” Solid State Communications 79.2 (1991) 143-146.

31. Kono, S., T. Goto, Y. Ogura, T. Abukawa, “ Surface electromigration of metals on Si(001): In/Si(001).” Surface Science 420 (1999) 200-212.

32. Dekker, J. P., A. Lodder. “Theory for the electromigration wind force in dilute alloys.” Physical Review B 56.19 (1997) 167-177.

33. Persad, C. “Railgun Tribology: Chemical Reactions between Contacts.” IEEE Transactions on Magnetics, in press, (2007).

THIS PAGE INTENTIONALLY LEFT BLANK

INITIAL DISTRIBUTION LIST

1. Defense Technical Information Center
   Ft. Belvoir, Virginia

2. Dudley Knox Library
   Naval Postgraduate School
   Monterey, California